# Earthquakes in Italy

L'Aquila

SR17ter

SR615

Normal fault

Fault plane

Reverse fault

Extension

Shortening

BEFORE FAULTING

DIP-SLIP FAULTS

Left-lateral fault

STRIKE-SLIP FAULT

OBLIQUE-SLIP FAULT

Here is an example of several main types of seismic waves. Our seismograph at Lillooet, B.C. recorded these waves from a magnitude 6.6 earthquake that occurred 600 km to the west on Nov. 2, 2004.

Time unfolds from left to right in the diagram, at a rate of 60 seconds per tick mark at the bottom, and the three traces indicate vibration of the earth vertically ("V") and in north-south ("N") and east-west ("E") directions.
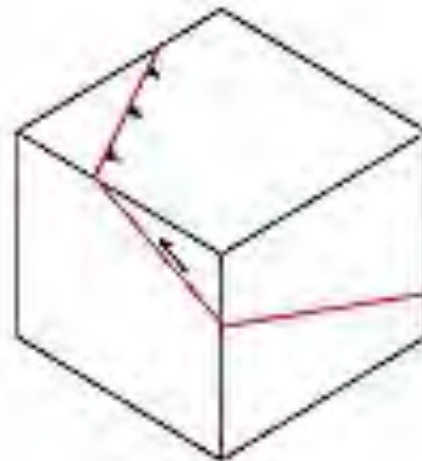
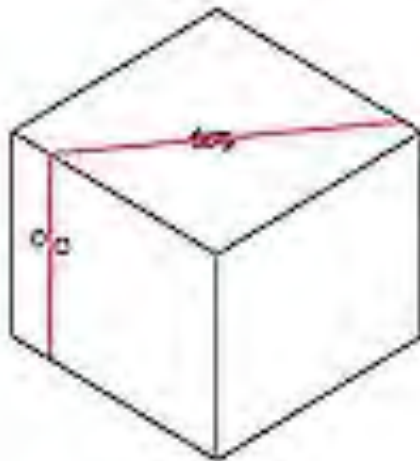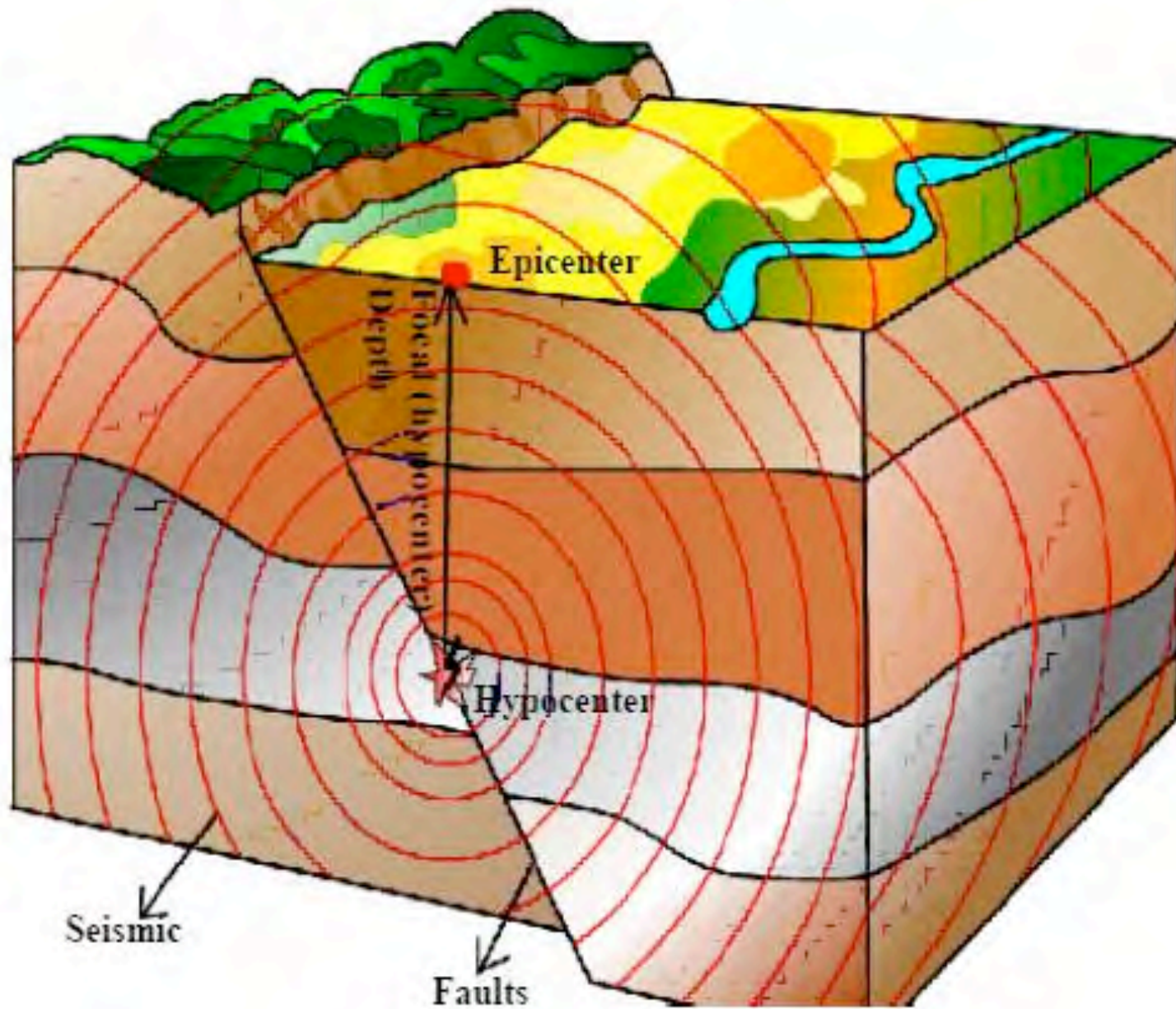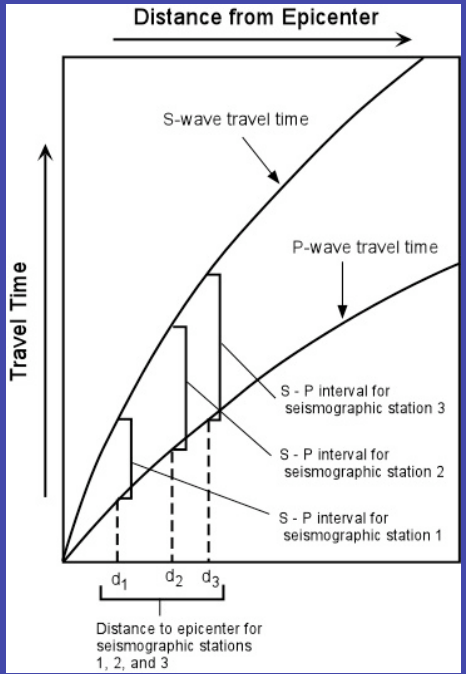Types of 'beachball plot' associated with different fault end-members
(nodal plane in red parallel to fault)

Strike-slip    Thrust    Normal

Stockholm

Honolulu

Kobe (epicenter)

Manila

V

R

P S

N

E

60 sec

**Distance from Epicenter**

S-wave travel time

P-wave travel time

Travel Time

S - P interval for
seismographic station 3

S - P interval for
seismographic station 2

S - P interval for
seismographic station 1

d₁ d₂ d₃

Distance to epicenter for
seismographic stations
1, 2, and 3

http://academic.brooklyn.cuny.edu/geology/grocha/plates/images/triangulation.jpg

http://earthsci.org/education/teacher/basicgeol/eartho/travtime.gif

# 6 April 2009 L'Aquila Earthquake
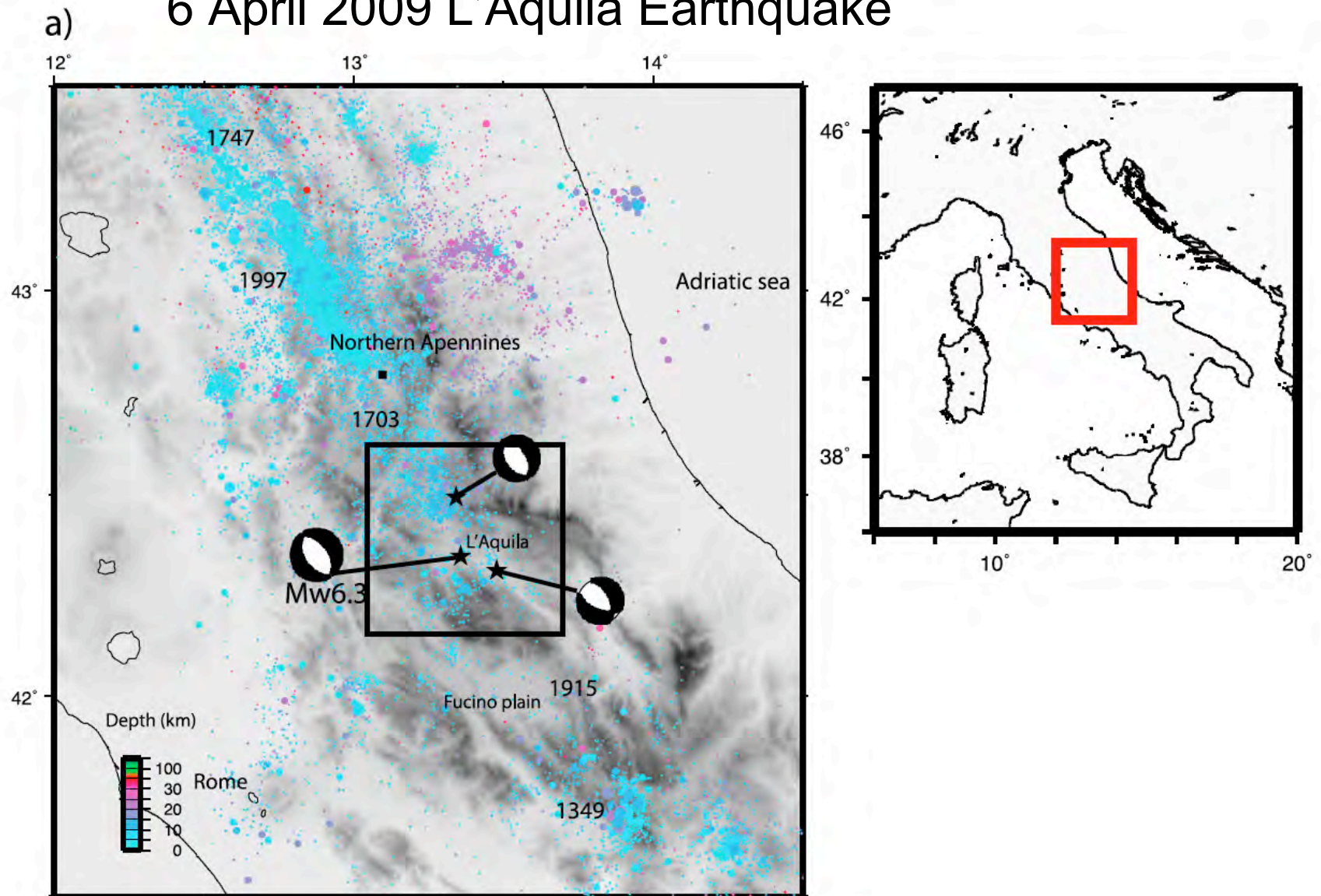


**Figure 1.** (a) Map of instrumental seismicity in the period 1980–2009, from the CSI catalogue. The L'Aquila sequence occurred in a silent region at the southern end of the Northern Apennines extensional belt. The stars indicate the three $M_L > 5$ earthquakes and the box is the area shown in Figure 2, focal mechanisms from the RCMT catalog (www.bo.ingv.it/RCMT).

(b) Space time distribution of the seismicity along this portion of the NW-trending extensional belt from April 2009. The dates of the most recent h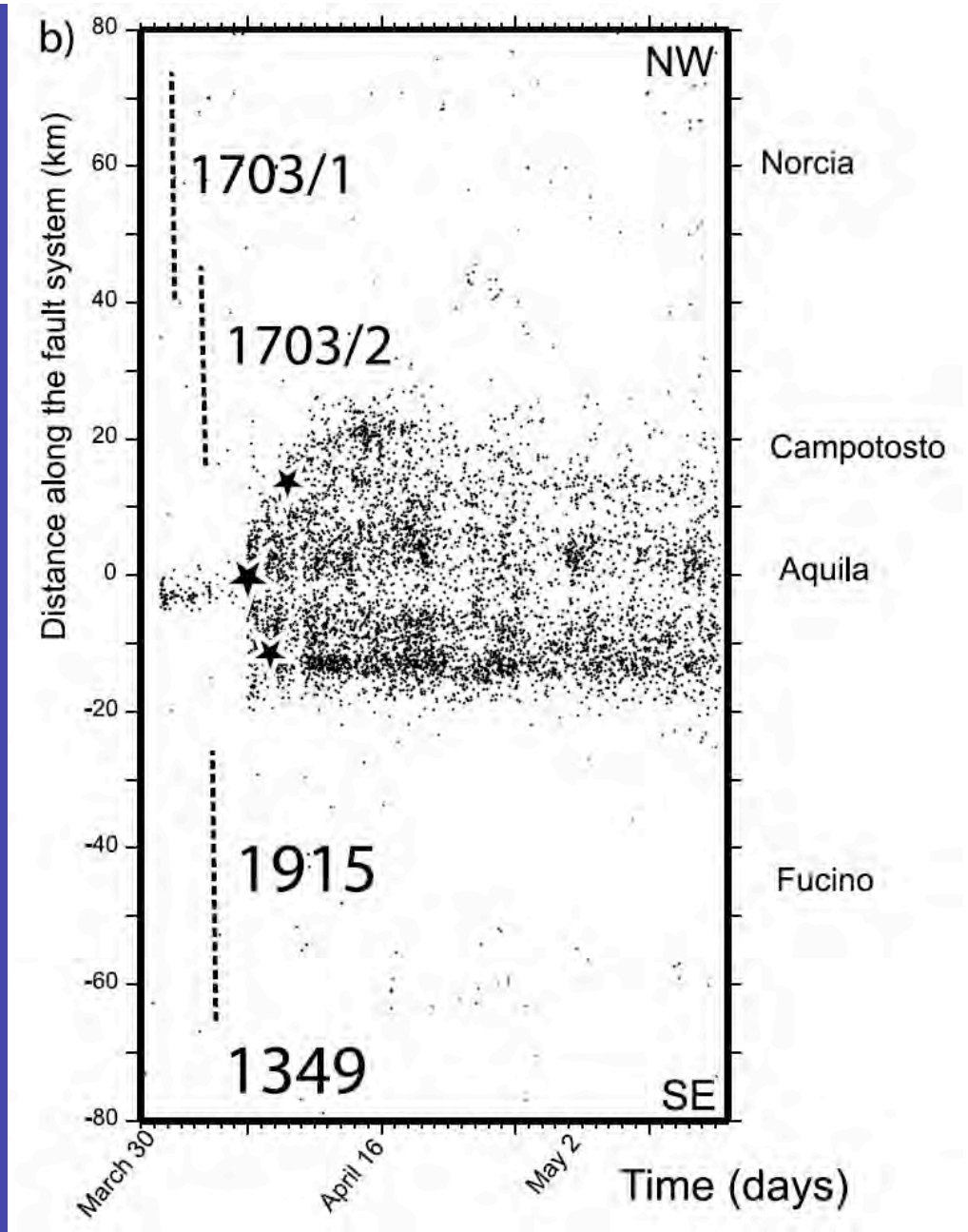istorical events are reported for each segment. (c) $M_L$ vs. time for the sequence starting at the end of March. The violet points are the 712 aftershocks re-analyzed in this work.
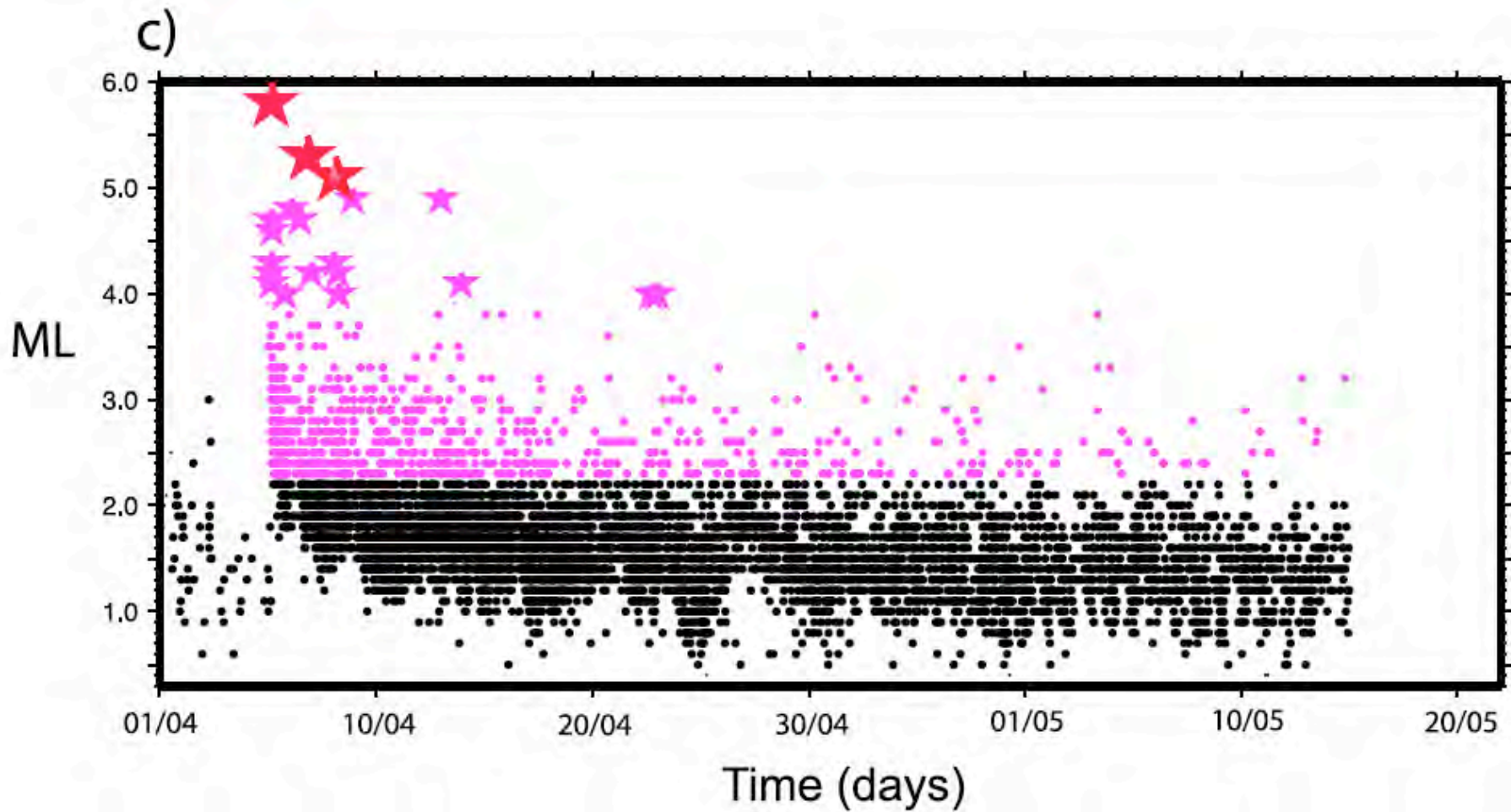
(b) Space time distribution of the seismicity along this portion of the NW-trending extensional belt from April 2009. The dates of the most recent historical events are reported for each segment. (c) $M_L$ vs. time for the sequence starting at the end of March. The violet points are the 712 aftershocks re-analyzed in this work.

Chiarabba et al 2009
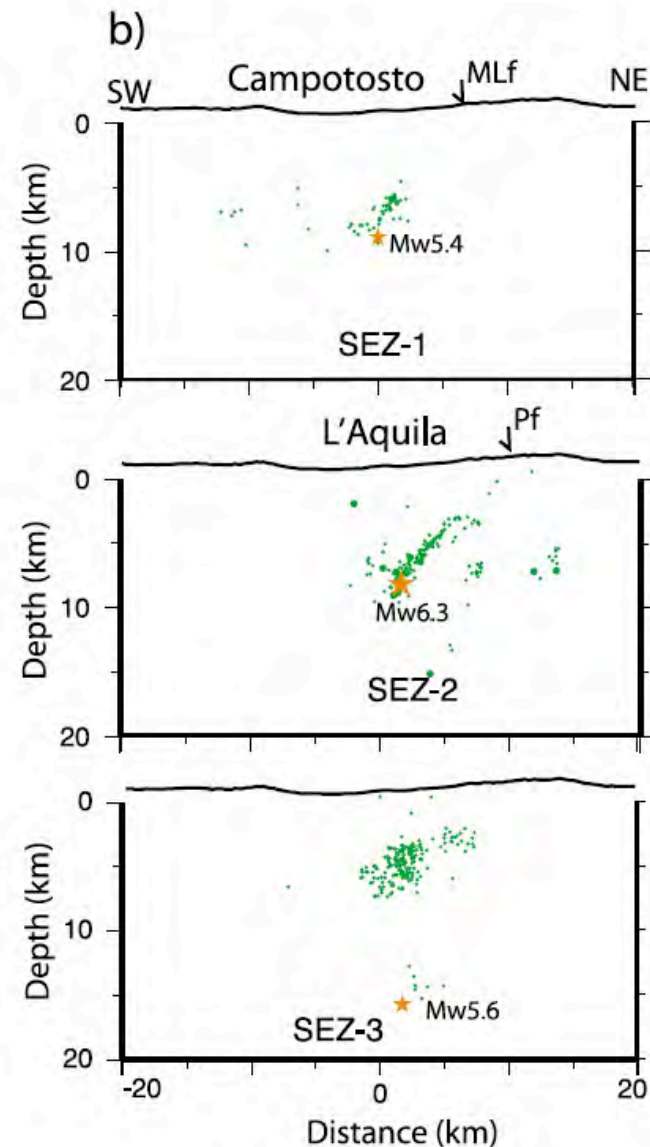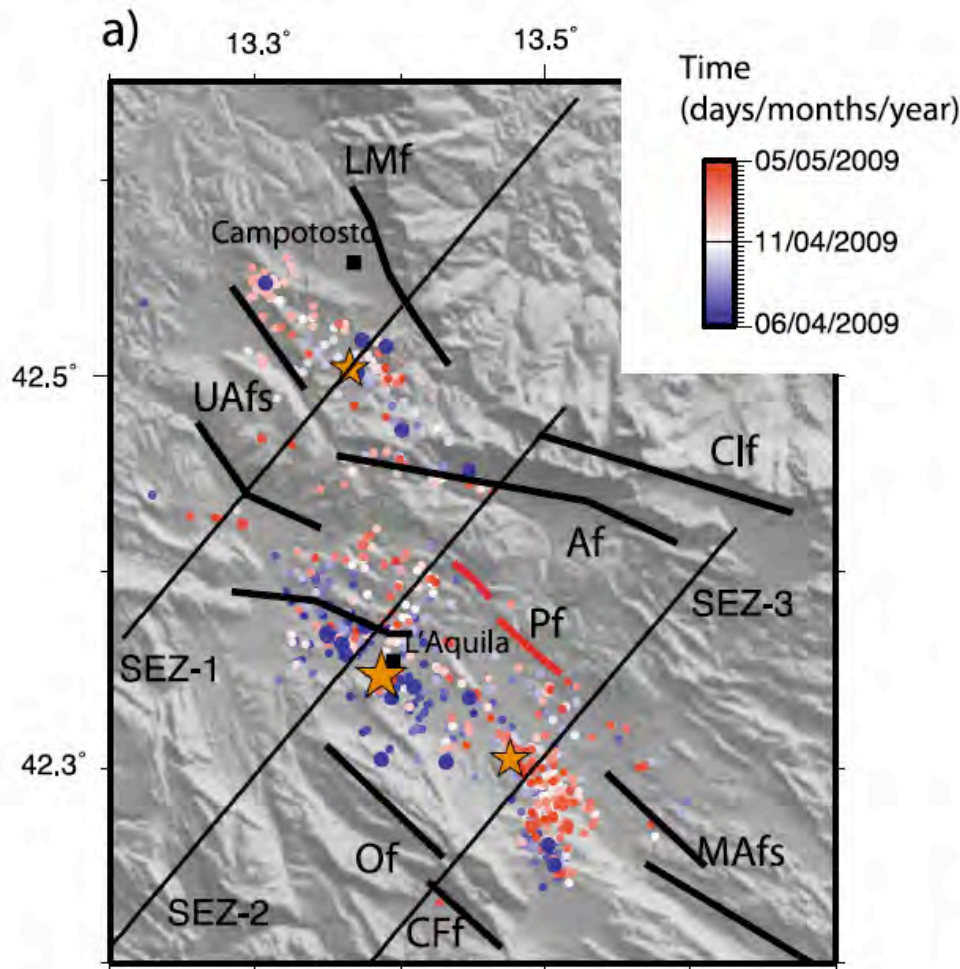
Chiarabba et al 2009

**Figure 2.** (a) Map of the 712 relocated events, with a color code indicating time after the main event. The dashed lines are the traces of vertical sections shown in Figure 2, and the solid lines are the mapped Quaternary faults [*Barchi et al.*, 2000]: (LMf, Laga Mts. fault; UAfs, Upper Aterno fault system; Af, Assergi fault; CIf, Campo Imperatore fault; MAfs, Middle Aterno valley fault system; OPf, Ovindoli Pezza fault; CFf, Campo Felice fault; Of, Ocre fault; Pf, Paganica fault). The box is a projection of the ruptured main fault. (b) Vertical sections across the Laga Mts. fault (SEZ-1) and the Paganica fault (SEZ-2, and SEZ-3). The fault geometry is consistently defined by the largest aftershocks. (c) Vertical section along the fault system,

**Figure 2.** (a) Map of the 712 relocated events, with a color code indicating time after the main event. The dashed lines are the traces of vertical sections shown in Figure 2, and the solid lines are the mapped Quaternary faults [*Barchi et al.*, 2000]: (LMf, Laga Mts. fault; UAfs, Upper Aterno fault system; Af, Assergi fault; CIf, Campo Imperatore fault; MAfs, Middle Aterno valley fault system; OPf, Ovindoli Pezza fault; CFf, Campo Felice fault; Of, Ocre fault; Pf, Paganica fault). The box is a projection of the ruptured main fault. (b) Vertical sections across the Laga Mts. fault (SEZ-1) and the Paganica fault (SEZ-2, and SEZ-3). The fault geometry is consistently defined by the largest aftershocks. (c) Vertical section along the fault system,
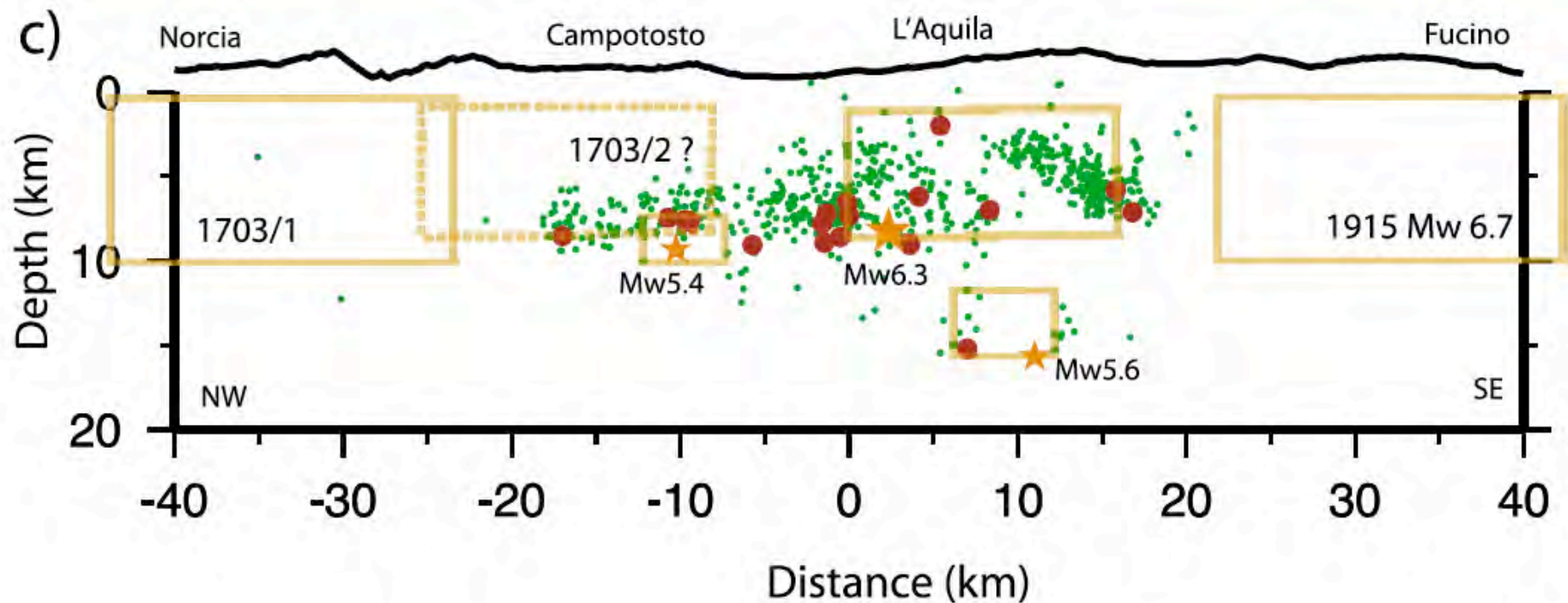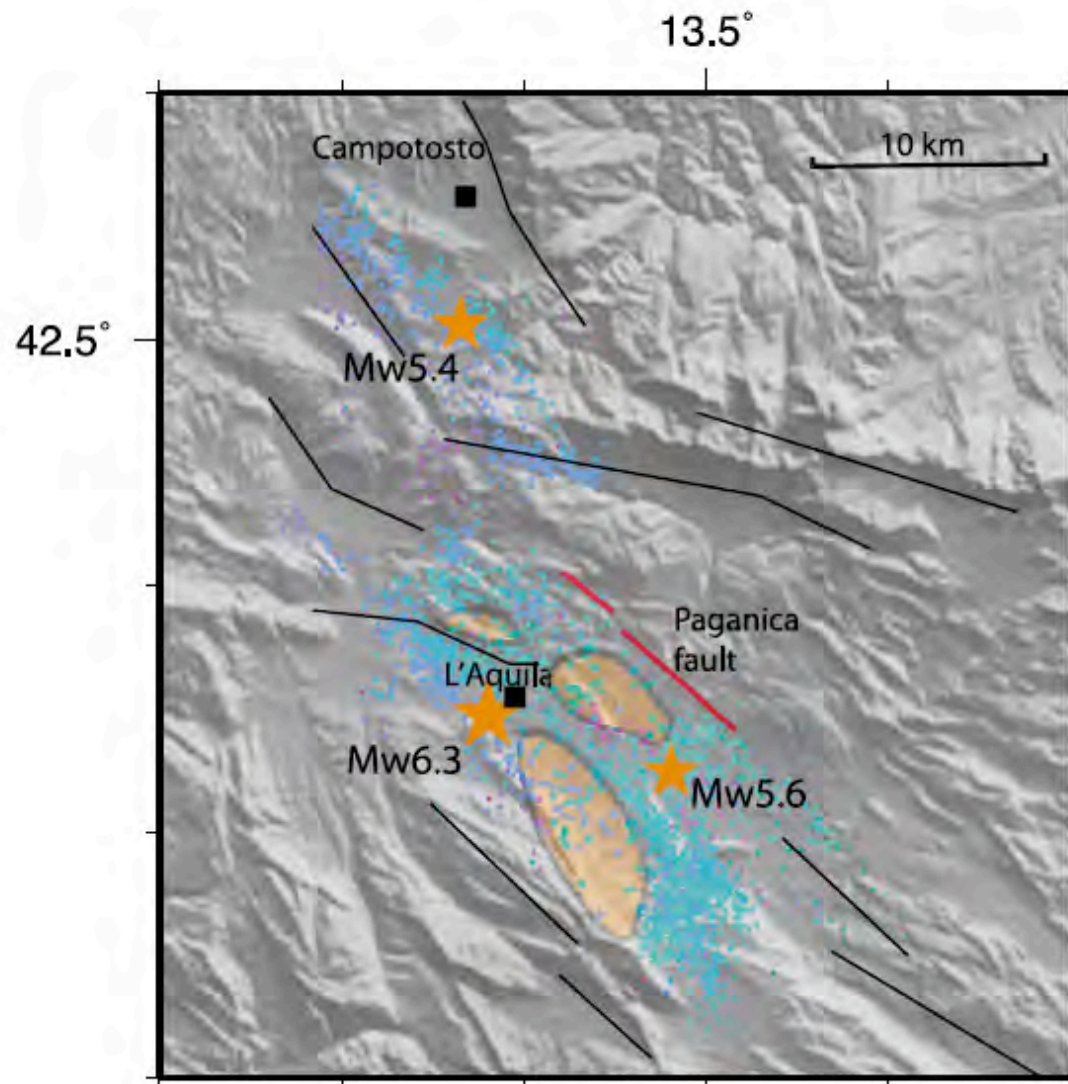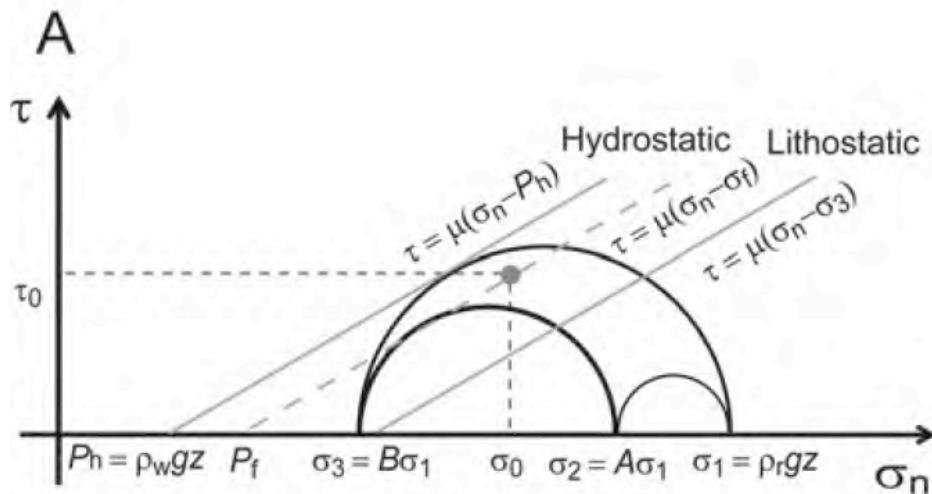
Chiarabba et al 2009

**Figure 3.** Map of the 3200 relocated events (see the auxiliary material) showing that aftershocks originate around three main patches that ruptured during the $M_W$ 6.3 event (orange shaded zones).

Chiarabba et al 2009

**A**

Hydrostatic   Lithostatic

$$\tau = \mu(\sigma_n - P_h)$$
$$\tau = \mu(\sigma_n - \sigma_f)$$
$$\tau = \mu(\sigma_n - \sigma_3)$$

$\tau_0$

$P_h = \rho_w g z$   $P_f$   $\sigma_3 = B\sigma_1$   $\sigma_0$   $\sigma_2 = A\sigma_1$   $\sigma_1 = \rho_r g z$   $\sigma_n$

$$\tau_s = \mu\left(\sigma_n - P_f\right) \qquad (1)$$

where $\tau_s$ is the shear strength, $\sigma_n$ is the normal stress, $P_f$ is the fluid pressure, and $\mu$ is the friction coefficient (taken as 0.6). The theory can be explained using a 3-D Mohr diagram (Fig. 2A).
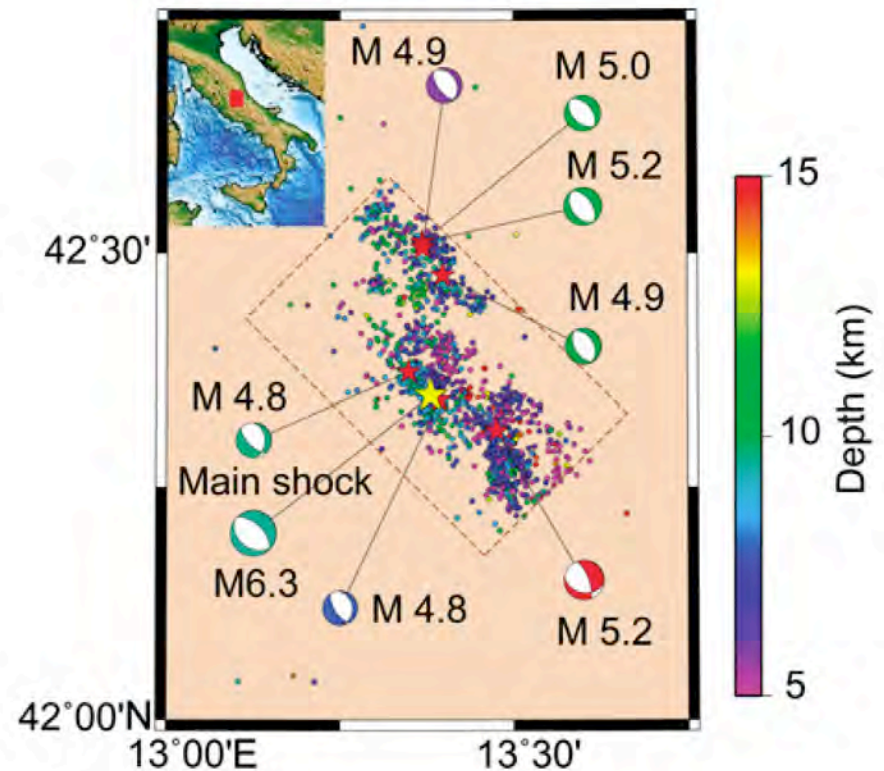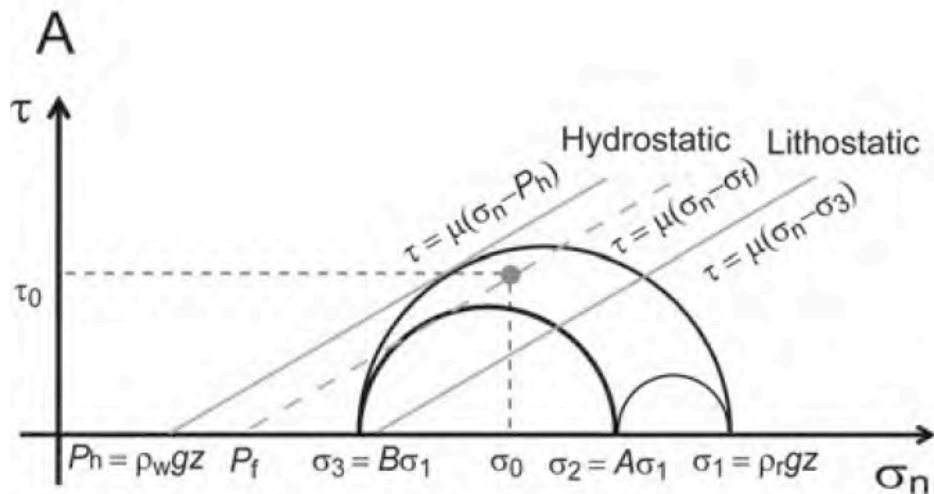


**Figure 1. Seismicity in the source region of the A.D. 2009 L'Aquila earthquake (Jan–July 2009). Hypocenters are shown as colored dots. Focal mechanisms of the main shock and large aftershocks are shown with the lower-hemisphere projection of focal spheres. Color of focal spheres and dots indicate depths of hypocenters. Model region is shown by the dashed rectangle.**

Terakawa et al 2010

## A

$$\tau_s = \mu(\sigma_n - P_f) \qquad (1)$$

where $\tau_s$ is the shear strength, $\sigma_n$ is the normal stress, $P_f$ is the fluid pressure, and $\mu$ is the friction coefficient (taken as 0.6). The theory can be explained using a 3-D Mohr diagram (Fig. 2A).
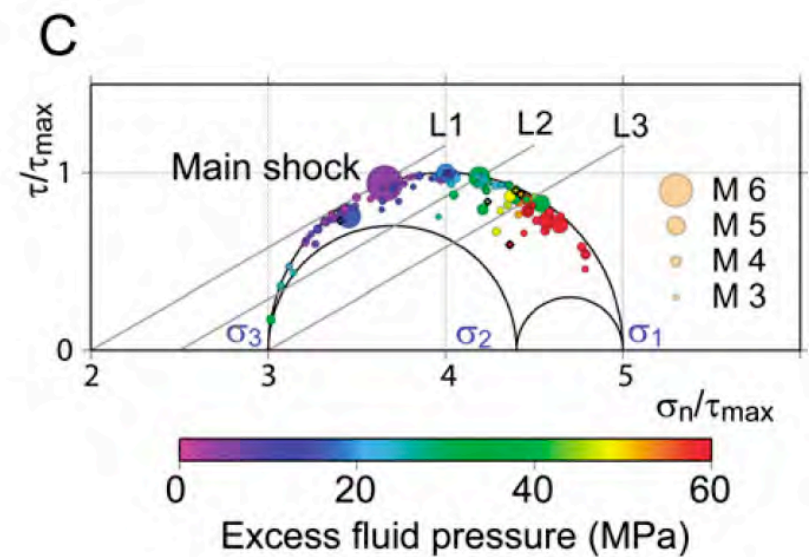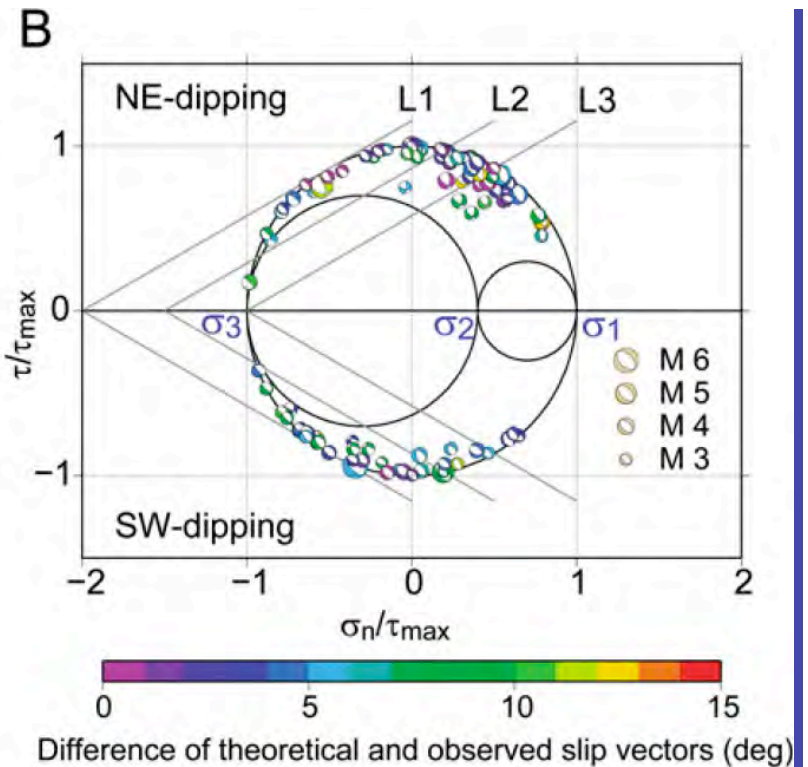
Terakawa et al 2010

Figure 2. Focal mechanism tomography (FMT) analysis. A: Theory of FMT. Horizontal and vertical axes show normal and shear stresses acting on fault planes. This is an example of extensional stress regime where $\sigma_1$, $\sigma_2$, and $\sigma_3$ are the maximum, intermediate, and minimum compressive principal stresses, respectively. Gray lines show fault strength for hydrostatic, intermediate, and lithostatic fluid pressures. B: Consistency of observed focal mechanisms (CT > 0.975) with the stress pattern. Focal mechanisms are shown in the Mohr diagram (normalized by the maximum shear stress with the lower-hemisphere projection of focal spheres, whose color indicates the misfit angle between the observed and theoretical slip vectors for events. Lines L1, L2, and L3 indicate fault strength under hydrostatic, intermediate, and lithostatic fluid pressures. C: Excess (above hydrostatic) fluid pressure associated with each event. Size of symbol (circles and diamonds represent aftershocks and foreshocks, respectively) scales with magnitude, and color indicates excess fluid pressure. Largest symbol shows the main shock. L1, L2, and L3 are the same as in B.
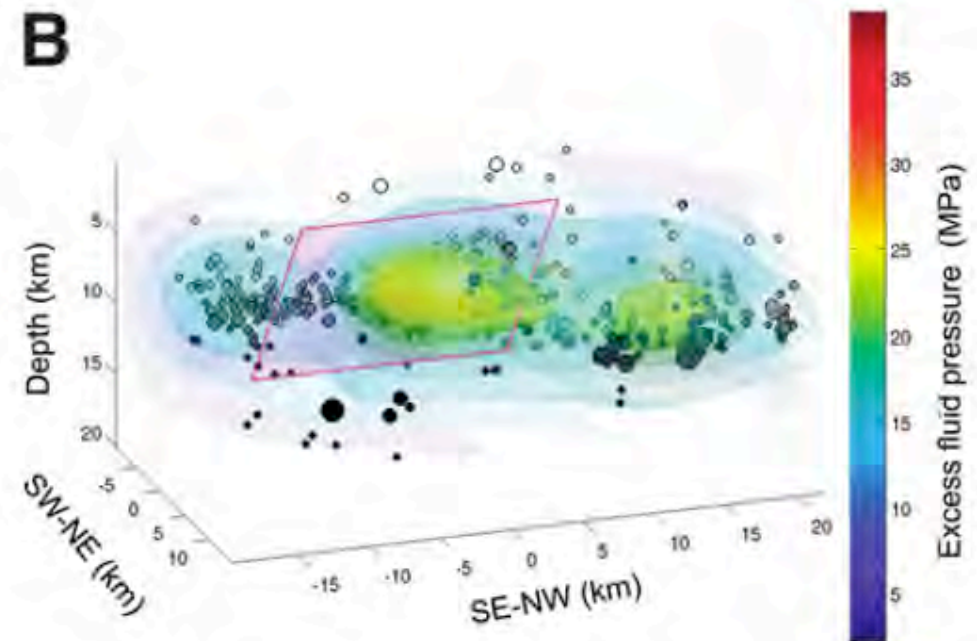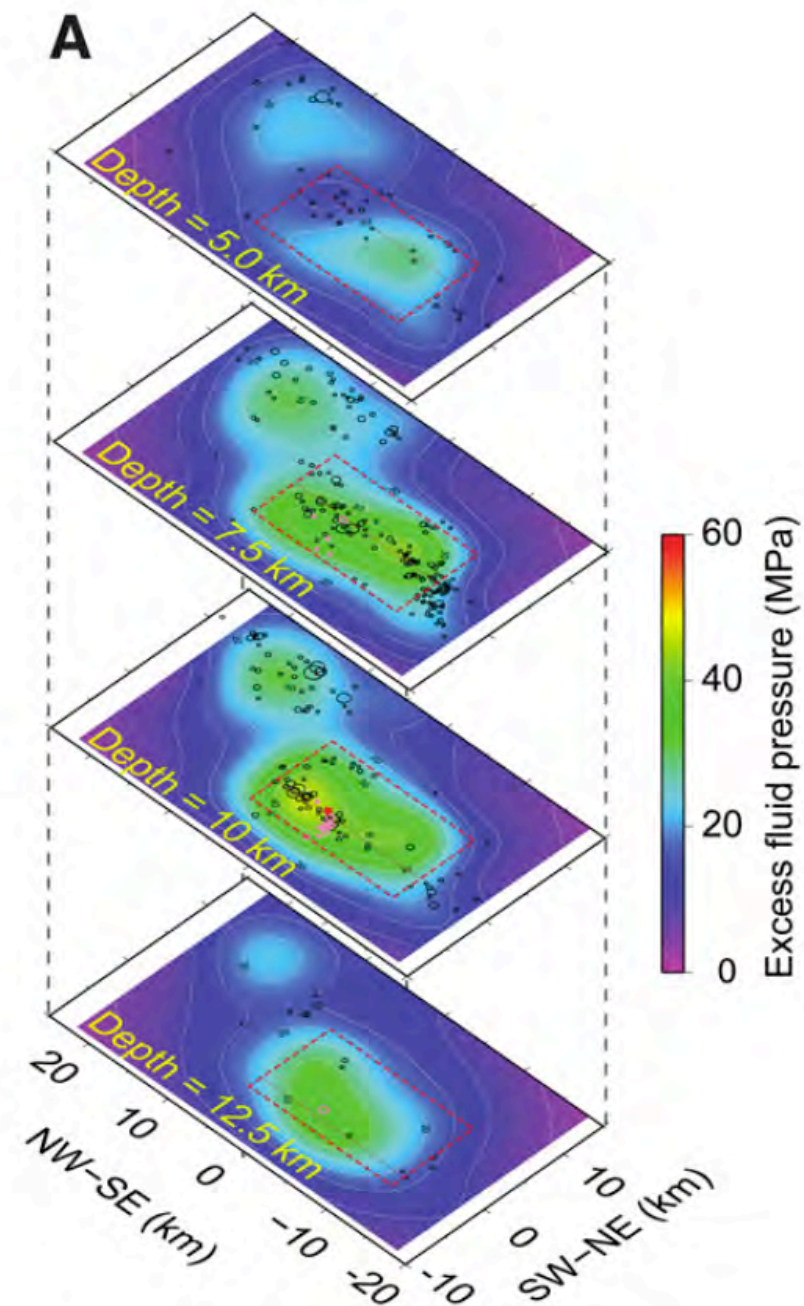
Terakawa et al 2010
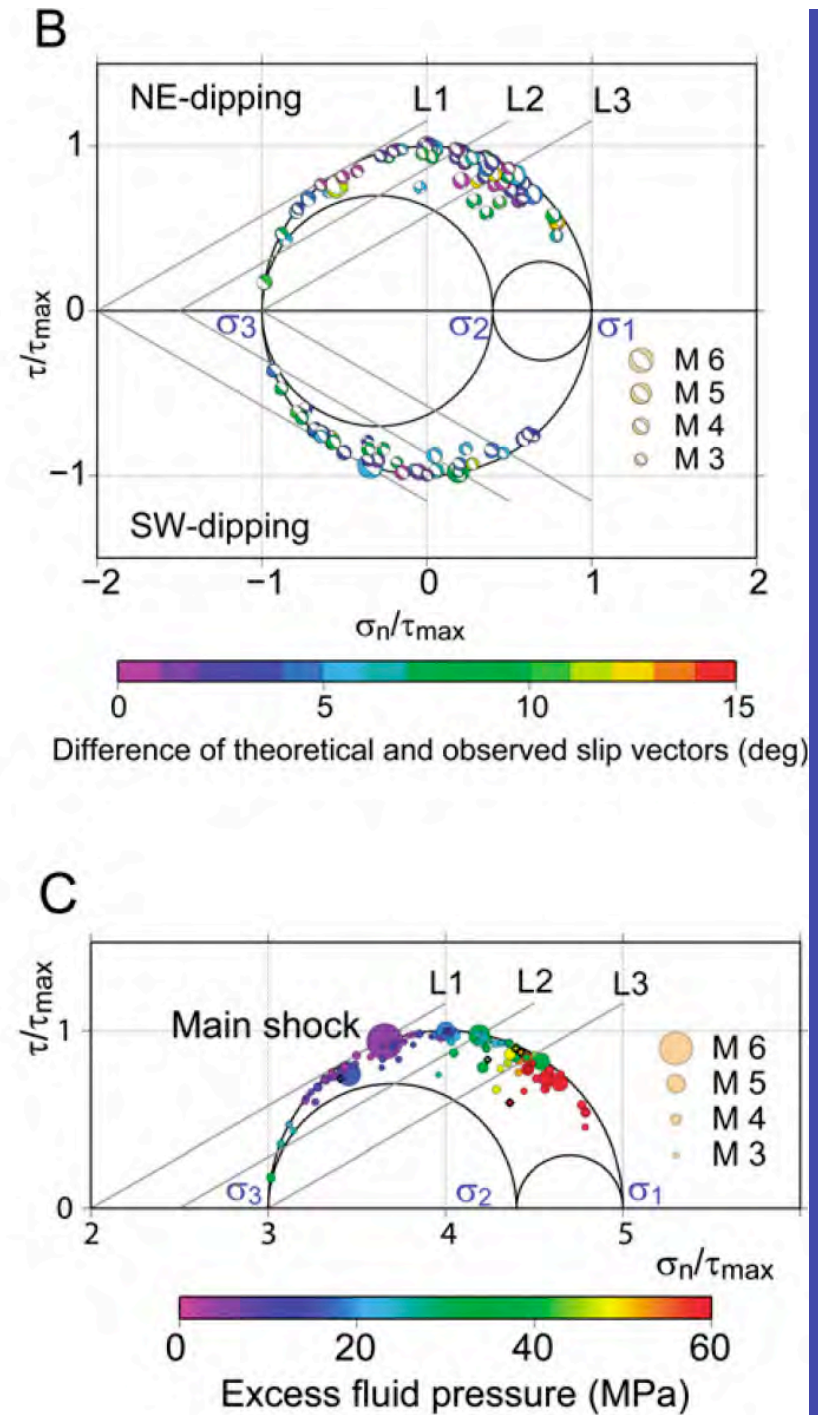
Figure 3. A: Map view of the excess fluid pressure distribution at depths of 5 km, 7.5 km, 10 km, and 12.5 km. All foreshocks and aftershocks (Chiarabba et al., 2009) with M ≥ 2.5 within 1 km of each plane (shown with pink and black circles, respectively) are superposed on the fluid pressure field. Red star indicates hypocenter of the main shock. Fault of the main shock (Cirella et al., 2009) is projected onto each plane. B: Three-dimensional image of the excess fluid pressure field with the hypocenters of foreshocks and aftershocks. View is from the northeast toward southwest.
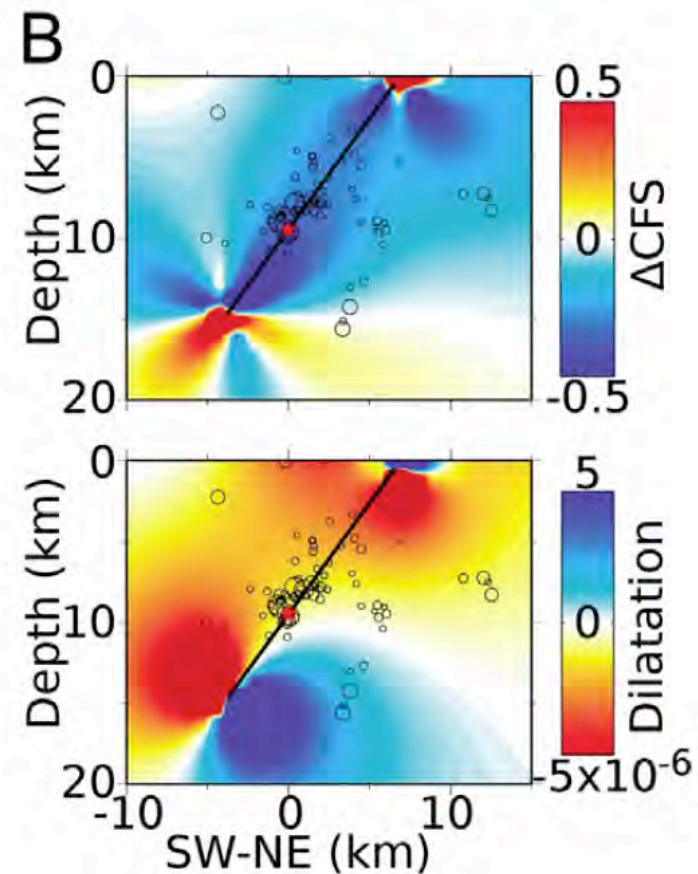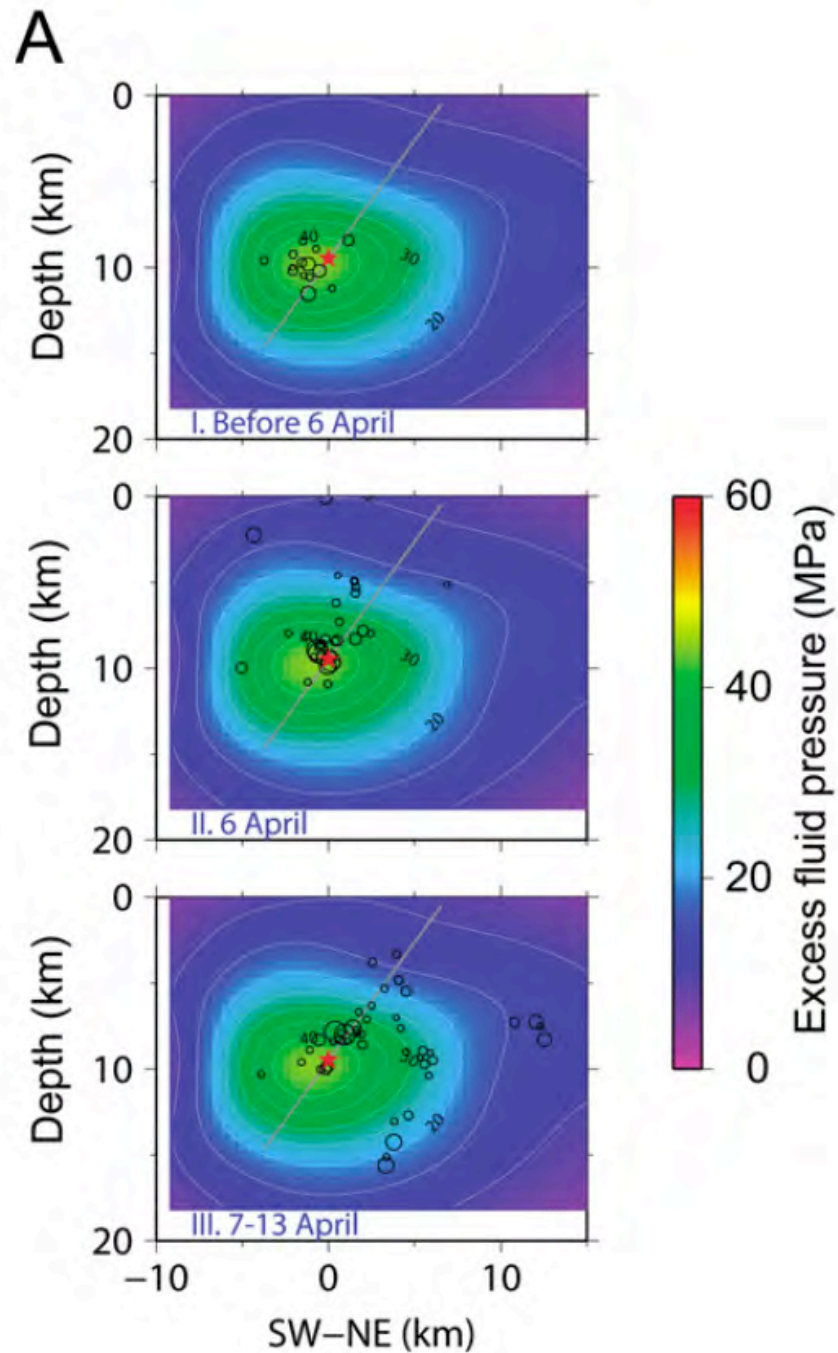
Terakawa et al 2010

Figure 4. Evolution of seismicity, and static stress and strain changes due to the main shock on the cross section (NE-SW) at the hypocenter. A: Seismicity superposed on the estimated fluid pressure field (I) before main shock, (II) on 6 April, and (III) on 7–13 April. Events (M > 2.5) within 5 km of the cross section are plotted. B: ΔCFS (upper panel) and dilatation (lower panel) due to main shock, assuming 0.25 m uniform slip on the main-shock fault (Cirella et al., 2009) in an elastic halfspace. Plotted events are the same in A.

Terakawa et al 2010
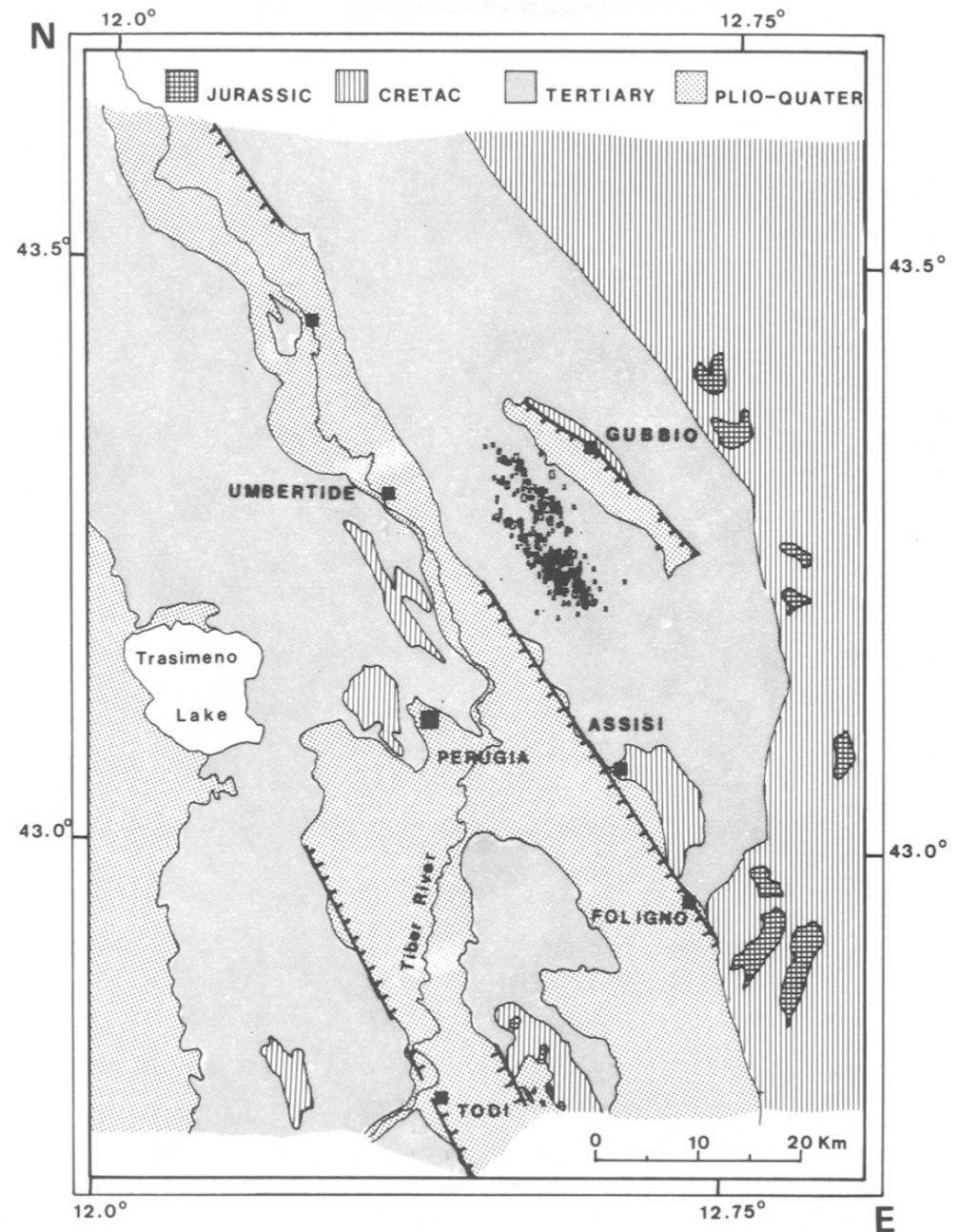
# 29 April 1984
# Perugia Earthquake



FIG. 2. Simplified geological scheme of the Perugia region displaying Plio-quaternary basins and recent faulting. Valleys are controlled by normal faulting. Aftershock clusters are located between Perugia and Gubbio and their trend is parallel to the orientation of the valleys and to the strike of the faults. Epicenters are represented by rectangles whose size increases with the magnitude.
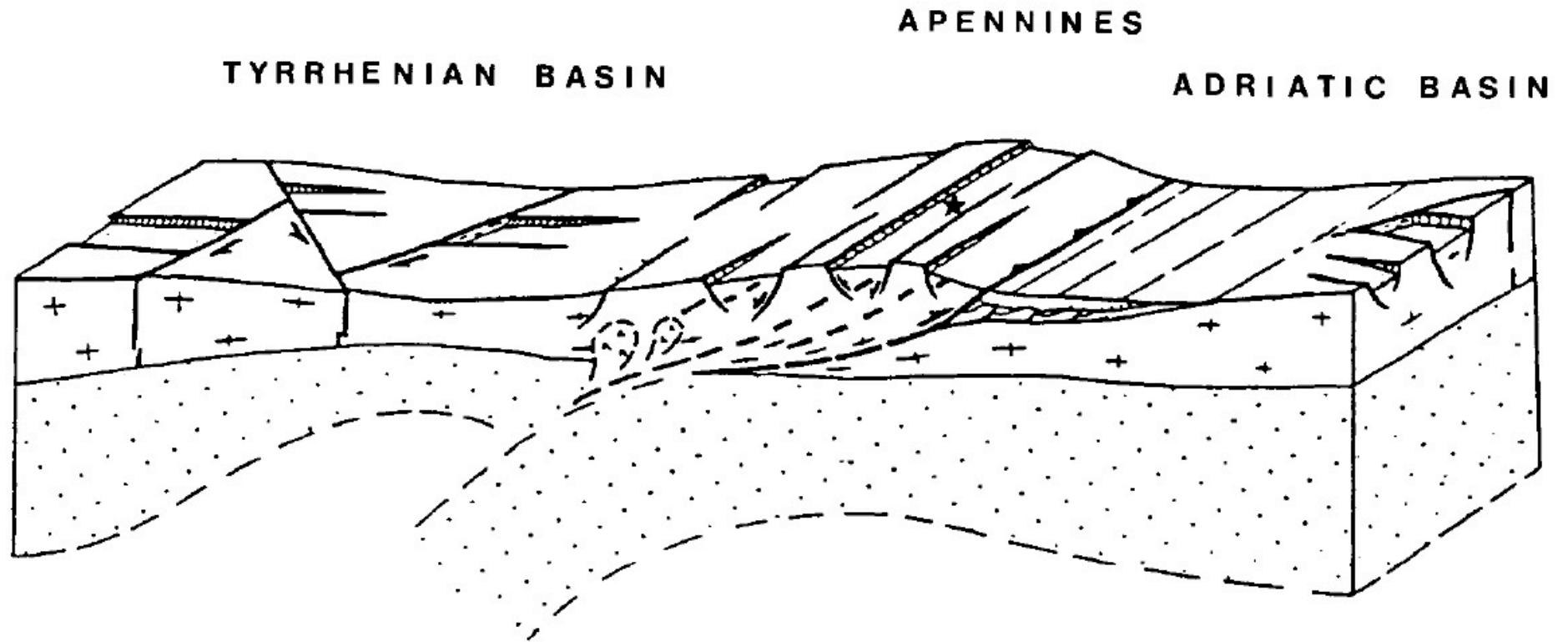
Haessler et al 1988

FIG. 3. Schematic block diagram across Perugia showing continental subduction (after Bousquet and Philip, 1986). Crosses correspond to crustal material and dots to the lithospheric mantle. The Moho level shows crustal thickening at the collision front. On the contrary, the crust is thinner where extension took place. An accretion prism is observed in the Adriatic basin. The star shows the relative position of the Perugia earthquake.
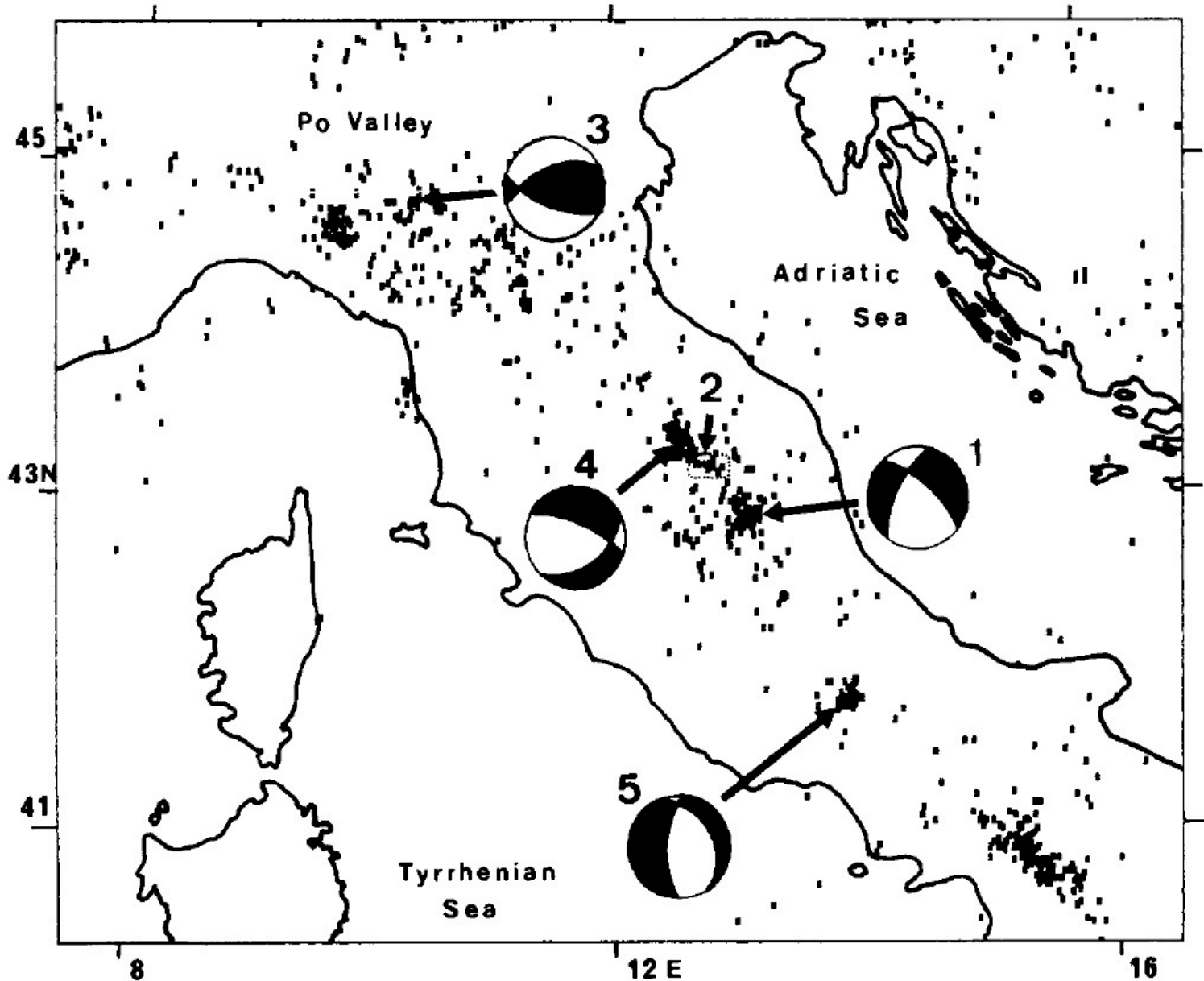
Haessler et al 1988

FIG. 4. Recent seismicity of central Italy (1976–1985). Data from the Euro-Mediterranean Seismological Center (EMSC). The focal mechanisms are those of Figure 7. 1. Norcia 1979. 2. Assisi sequence of 1982. 3. Parma 1983. 4. Perugia 1984. 5. Abruzzi 1984.
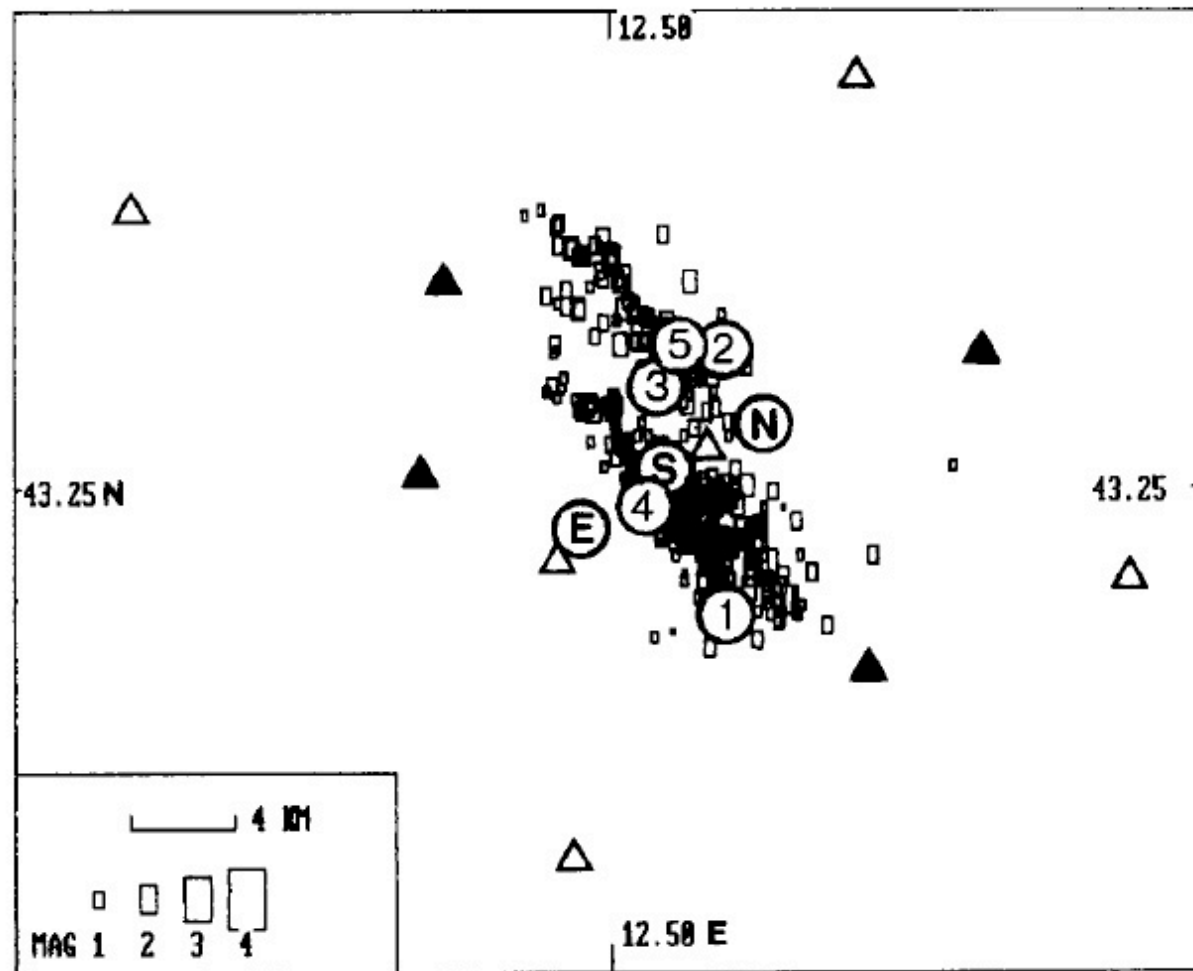
FIG. 6. Epicenters of aftershocks (rectangles) recorded from 6 May to 10 May 1984. Open circles with numbers are: the main shock (1), and the aftershocks (2), (3) and (4), of magnitude higher than 4 relocated using the 10 May 1984, 9:45 hrs shock ($M = 4.0$) as master event (5). Open circles with letters are main shock locations given by the international agencies, E: EMSC, N: NEIC, S: ISC. Open triangles are the MEQ stations and filled triangles are the GEOSTRAS digital stations. The aftershocks are distributed along two parallel clusters striking NW.
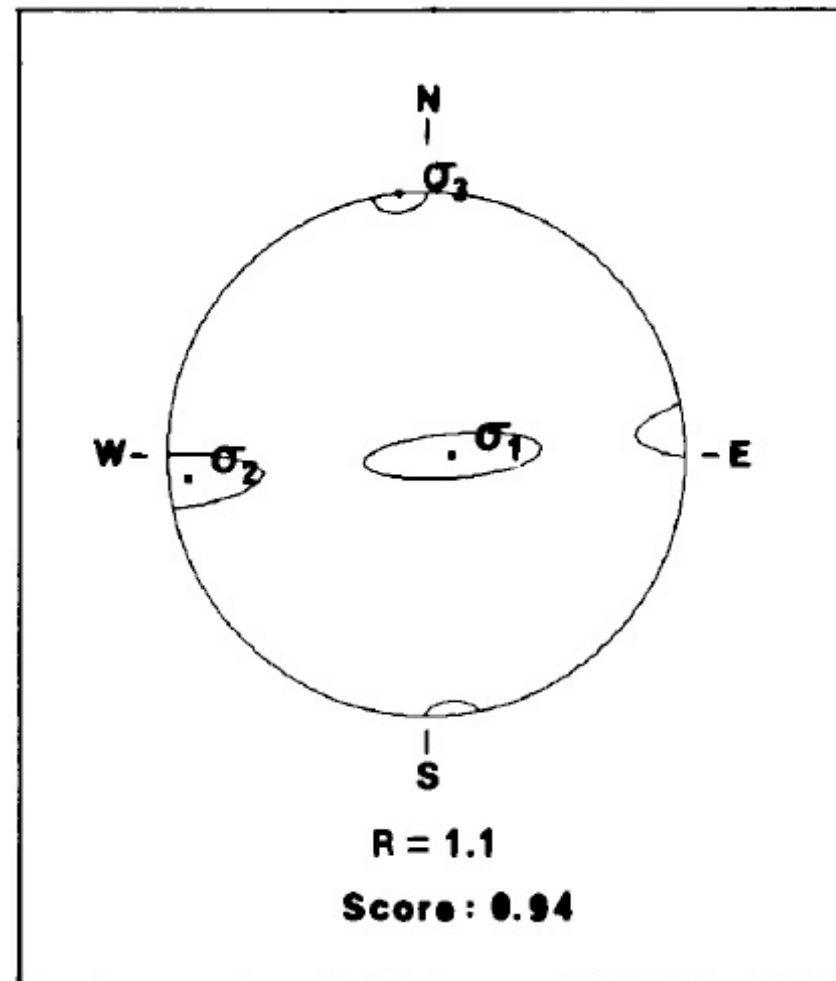
Haessler et al 1988

FIG. 10. Stress tensor orientation and shape factor $R$, for the Perugia 1984 aftershock sequence. Lower hemisphere Schmidt projection. The stress correspond to almost uniaxial extension with a NS oriented $\sigma_3$ axis. Confidence regions correspond to one standard deviation. The score is the percentage of consistent polarities.

Haessler et al 1988
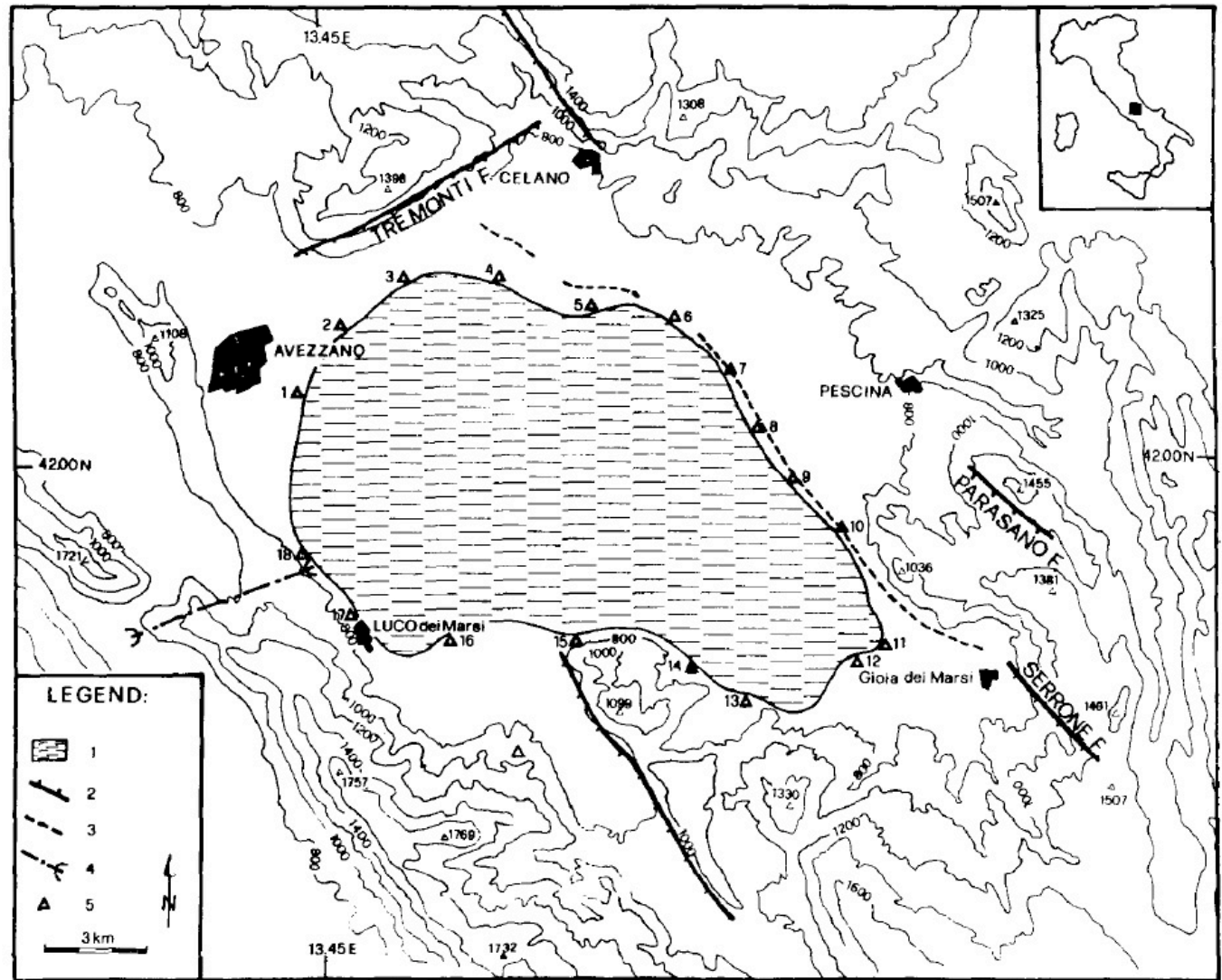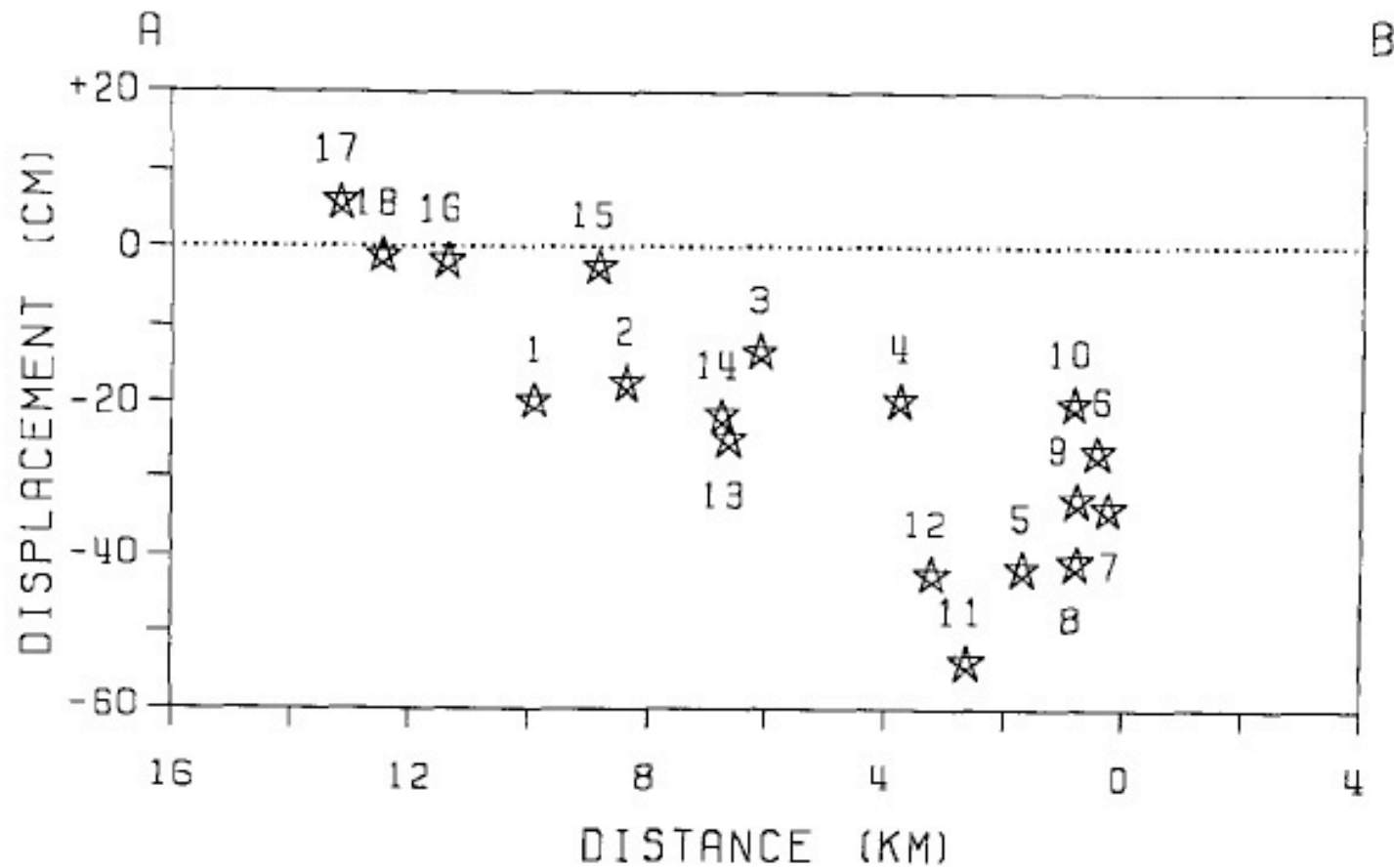
# 24 Jan 1915 Avezzano Earthquake

FIG. 1. (*Top*) Location map of the epicentral region of the 1915 Avezzano earthquake. Legend entries are: 1) Old Lake Bed, 2) Notable Quaternary and Holocene faults, 3) Scarp of 1915 event, 4) Roman Tunnel, and 5) Benchmark sites. (*Bottom*) Profile of the 1917 through 1862 vertical elevation changes projected along a line perpendicular to the Serrone Fault. The zero level is arbitrary. Total variance in the data is 1.4 m².

Ward and Valensisei 1989

Tunnel, and 5) Benchmark sites. (*Bottom*) Profile of the 1917 through 1862 vertical elevation changes projected along a line perpendicular to the Serrone Fault. The zero level is arbitrary. Total variance in the data is 1.4 m².
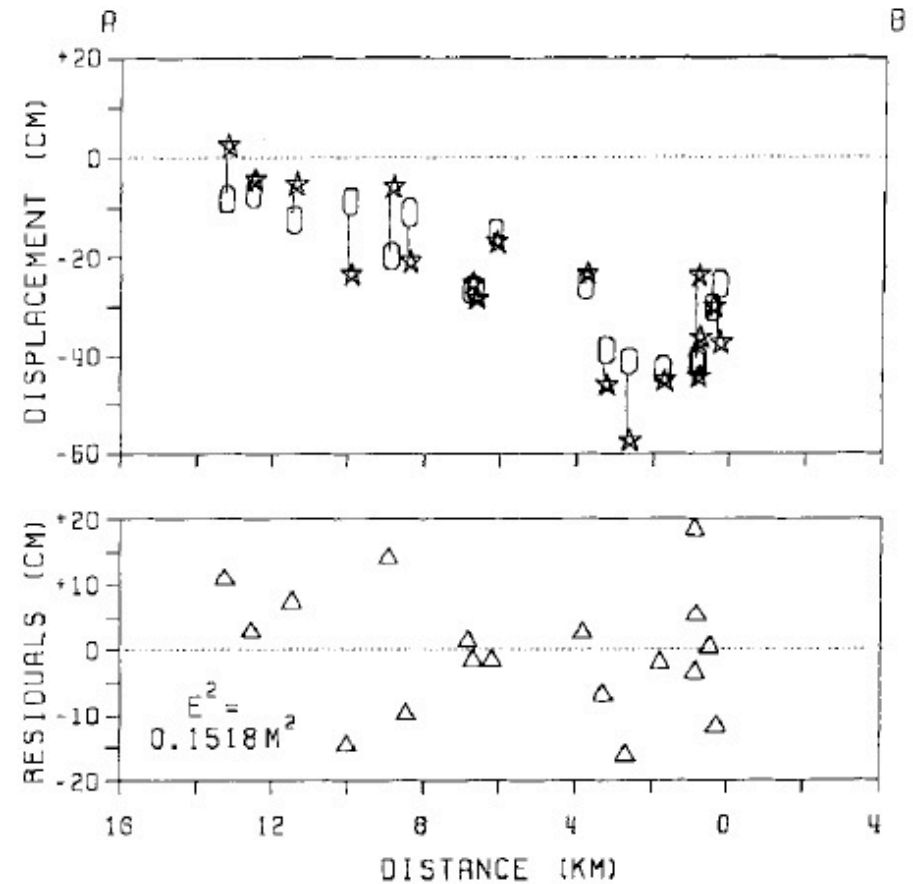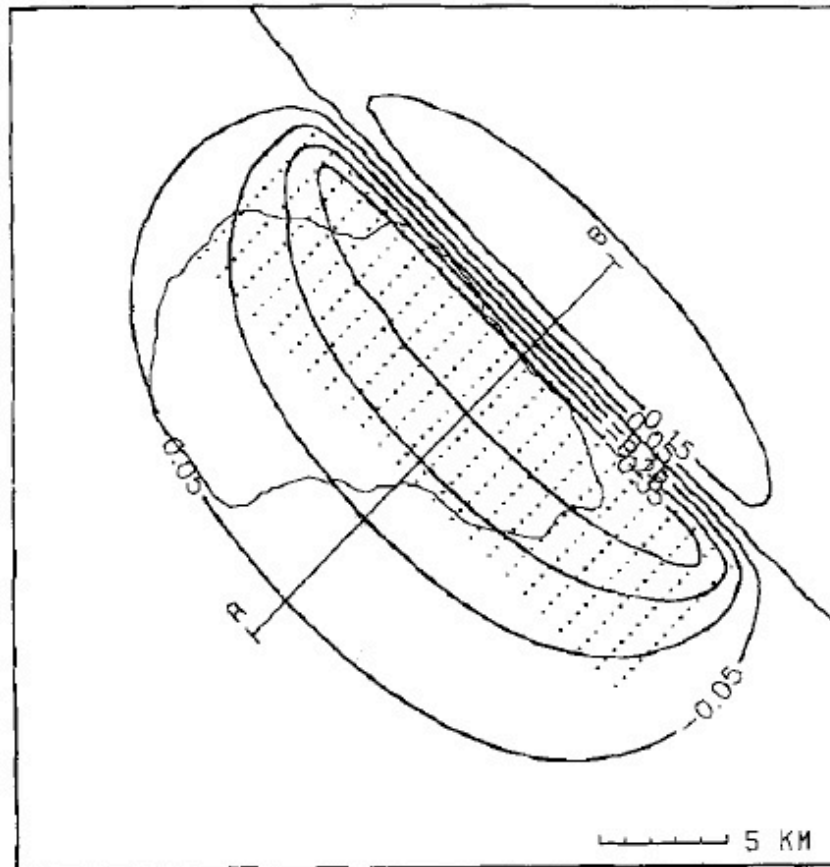


Ward and Valensisei 1989

FIG. 2. (*Left*) Contour map of vertical surface deformation at 0.1 m intervals for the best fitting rectangular USP fault. Light dots represent the surface projection of locations of nonzero slip. (*Right, top*) Observed (stars) and calculated (circles) elevation changes for the survey loop projected on A-B. The zero level here is fixed by the inversion. (*Right, bottom*) Elevation residuals of the USP model projected along A-B. The USP model fits 90 per cent of the data variance, but has residuals about six times greater than the estimated survey noise.
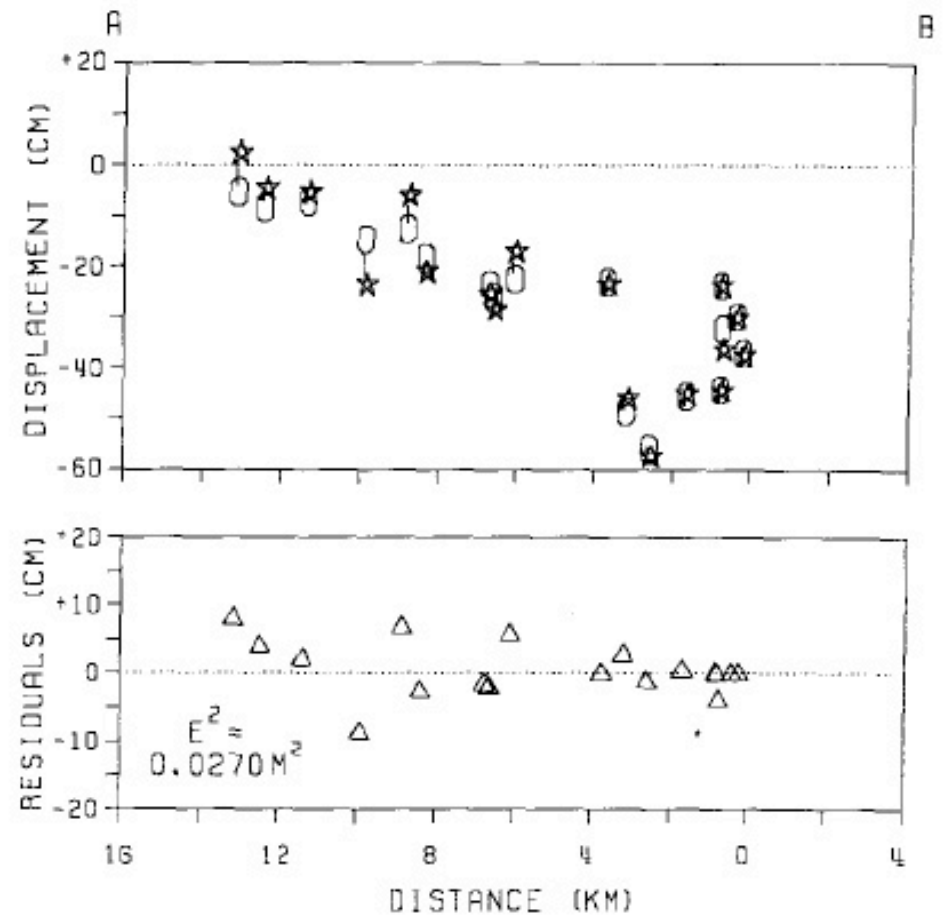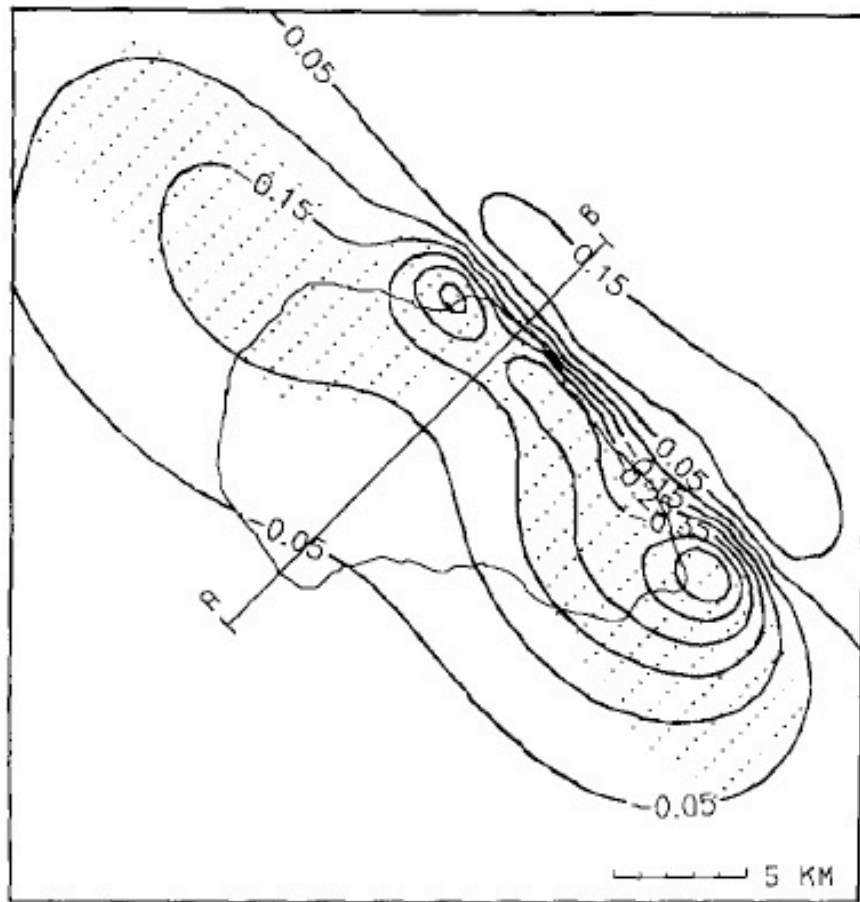
Ward and Valensisei 1989

FIG. 8. (*Left*) Contour map of vertical surface deformation at 0.1 m intervals for the VSP model of Figure 7. Light dots represent the surface projection of locations of non-zero slip. (*Right*) Observed and theoretical vertical displacements (*top*) and VSP residuals (*bottom*) projected along A-B. Summed square error (0.027 m²) is six times less than the best USP fit and about 4 per cent more than the expected survey error.
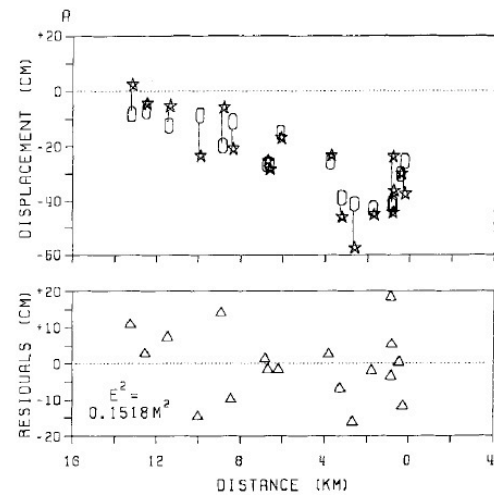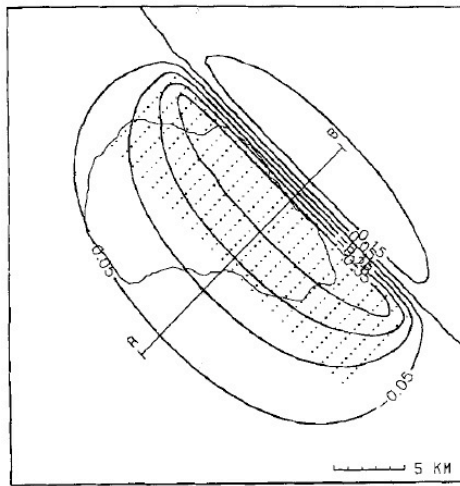
Ward and Valensisei 1989

FIG. 2. (*Left*) Contour map of vertical surface deformation at 0.1 m intervals for the best fitting rectangular USP fault. Light dots represent the surface projection of locations of nonzero slip. (*Right, top*) Observed (stars) and calculated (circles) elevation changes for the survey loop projected on A-B. The zero level here is fixed by the inversion. (*Right, bottom*) Elevation residuals of the USP model projected along A-B. The USP model fits 90 per cent of the data variance, but has residuals about six times greater than the estimated survey noise.
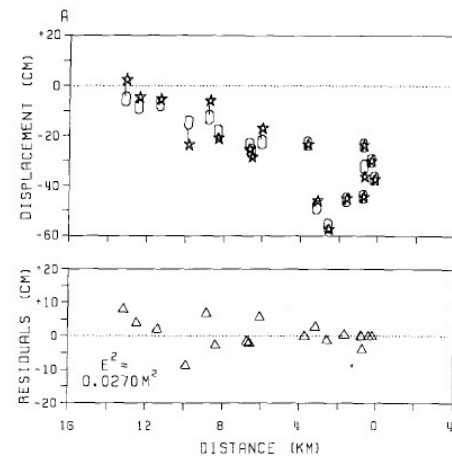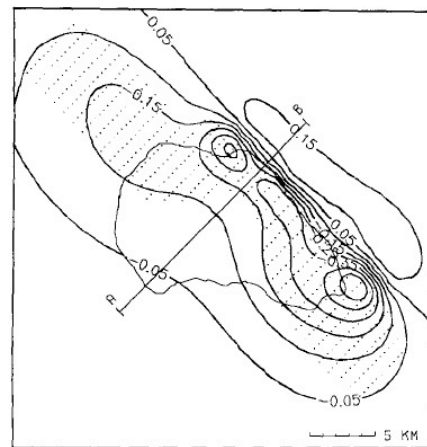


FIG. 8. (*Left*) Contour map of vertical surface deformation at 0.1 m intervals for the VSP model of Figure 7. Light dots represent the surface projection of locations of non-zero slip. (*Right*) Observed and theoretical vertical displacements (*top*) and VSP residuals (*bottom*) projected along A-B. Summed square error (0.027 m²) is six times less than the best USP fit and about 4 per cent more than the expected survey error.
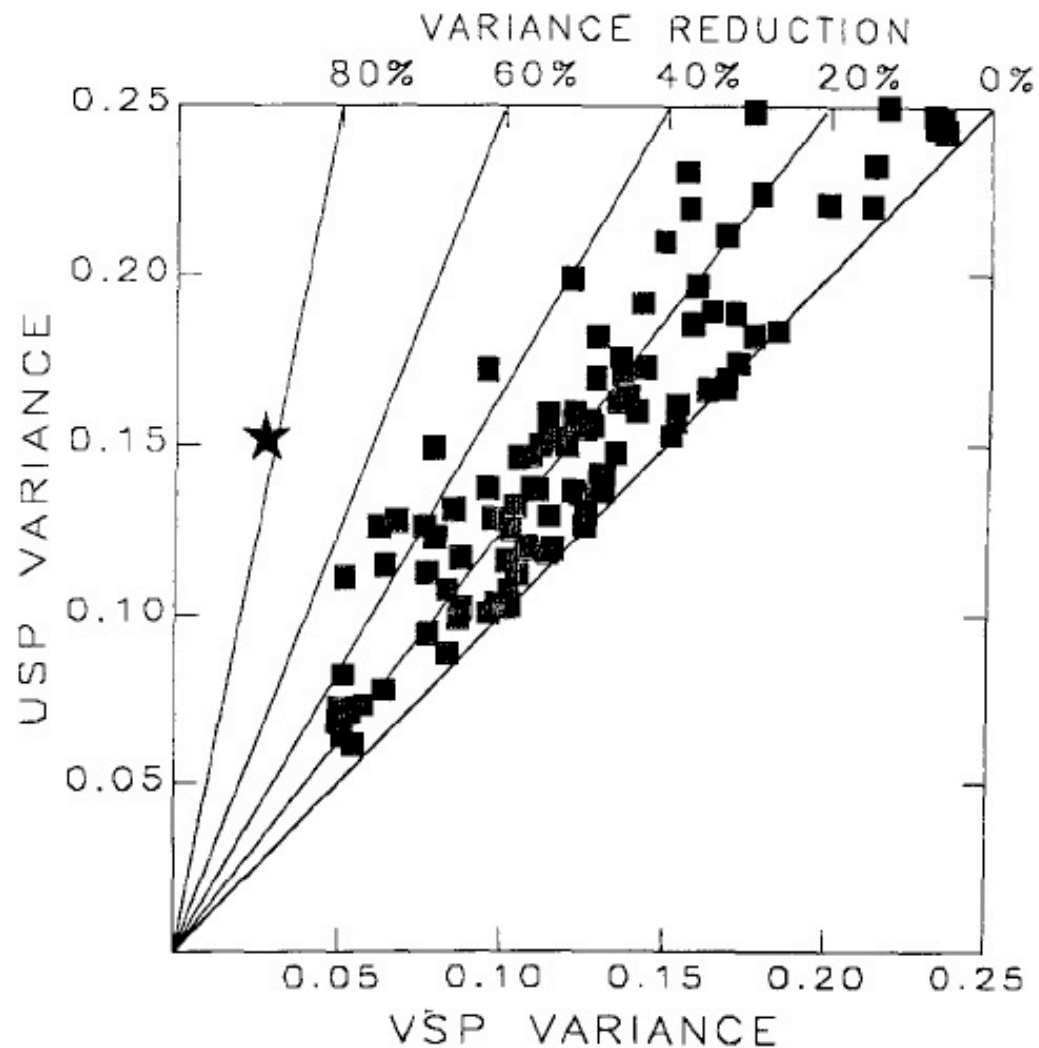
Ward and Valensisei 1989

FIG. 14. Plot of VSP versus USP variance for the real data (large star) and 100 artifically generated sets of random residuals (squares). The VSP technique does not fit random data very well. The average variance reduction for the random sets was only 18 per cent. The large variance reduction in the actual set compared with the randomly generated ones suggests that the USP residuals, although small, do represent a systematic misfit of the leveling data.

Ward and Valensisei 1989

Throughout the world, the seismic potential of areas lacking recent earthquake activity is largely judged by the length and height of the surface expressions of mappable faults. Unfortunately, the practice is not foolproof, many authors (Bonilla *et al.*, 1984; Darragh and Bolt, 1987) have pointed out important discrepancies between the magnitude-moment estimates implied from purely geological evaluations and the measured strength of historical events. The discrepancies are probably due to the disparity between the length of faults measured at the surface and their actual dimensions, which is partially obscured by intervening cover. Variable slip analyses such as these are one of the few methods available that can reveal the spatial extent of faults that lack significant surface expression.

Ward and Valensisei 1989

28 Dec 1908 Messina Earthquake

60,000+ killed

Largest seismic event in Calabria since 1783.

12 meter high tsunami that moved 200+ m inland.

Capuano et al 1988

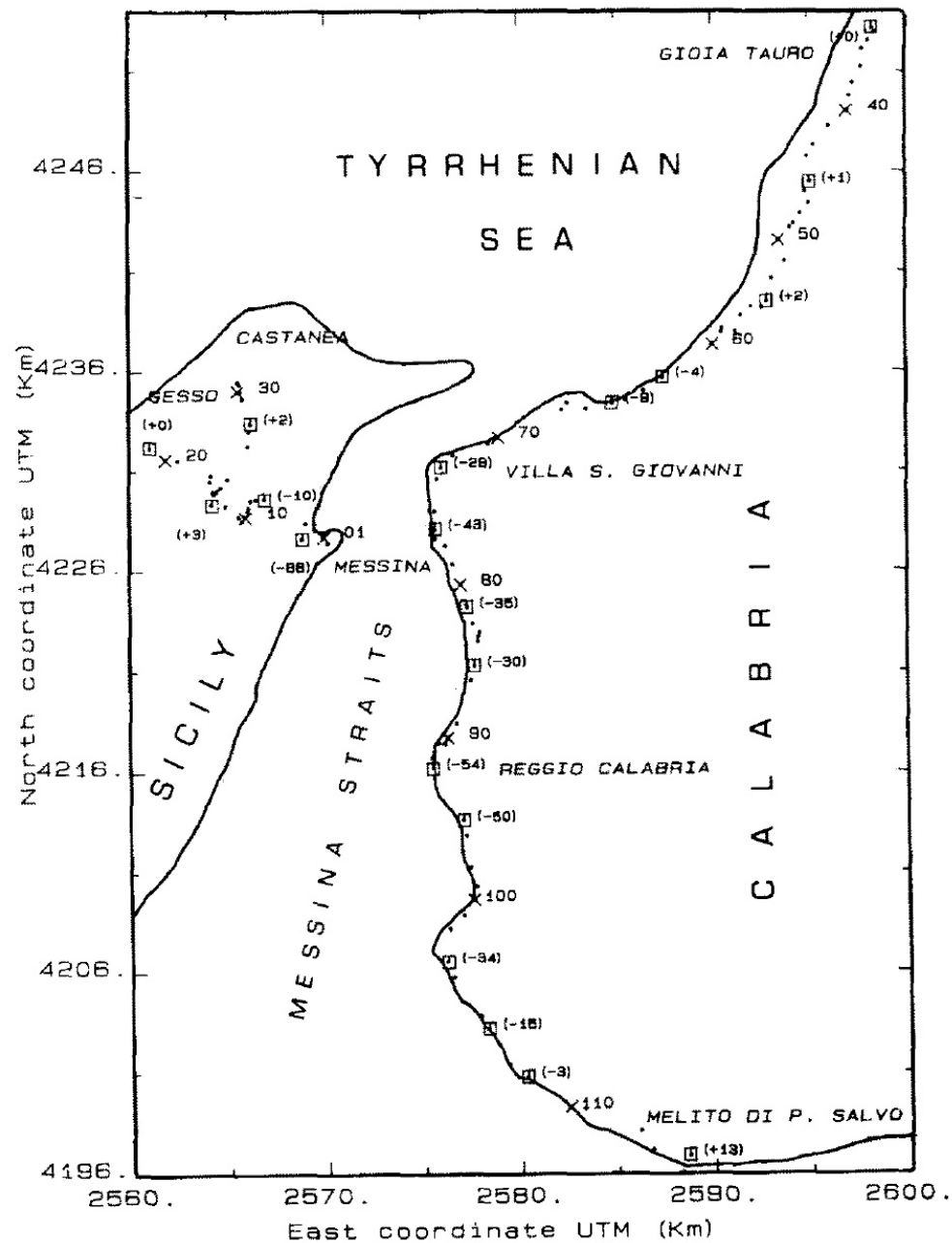MODEL FOR THE 1908 MESSINA STRAITS EARTHQUAKE    1931

FIG. 1. Levelling network (dots). Symbol "x" indicates numbered bench marks; some displacements (in cm) are also reported (in brackets), corresponding to bench marks indicated by ⊡.
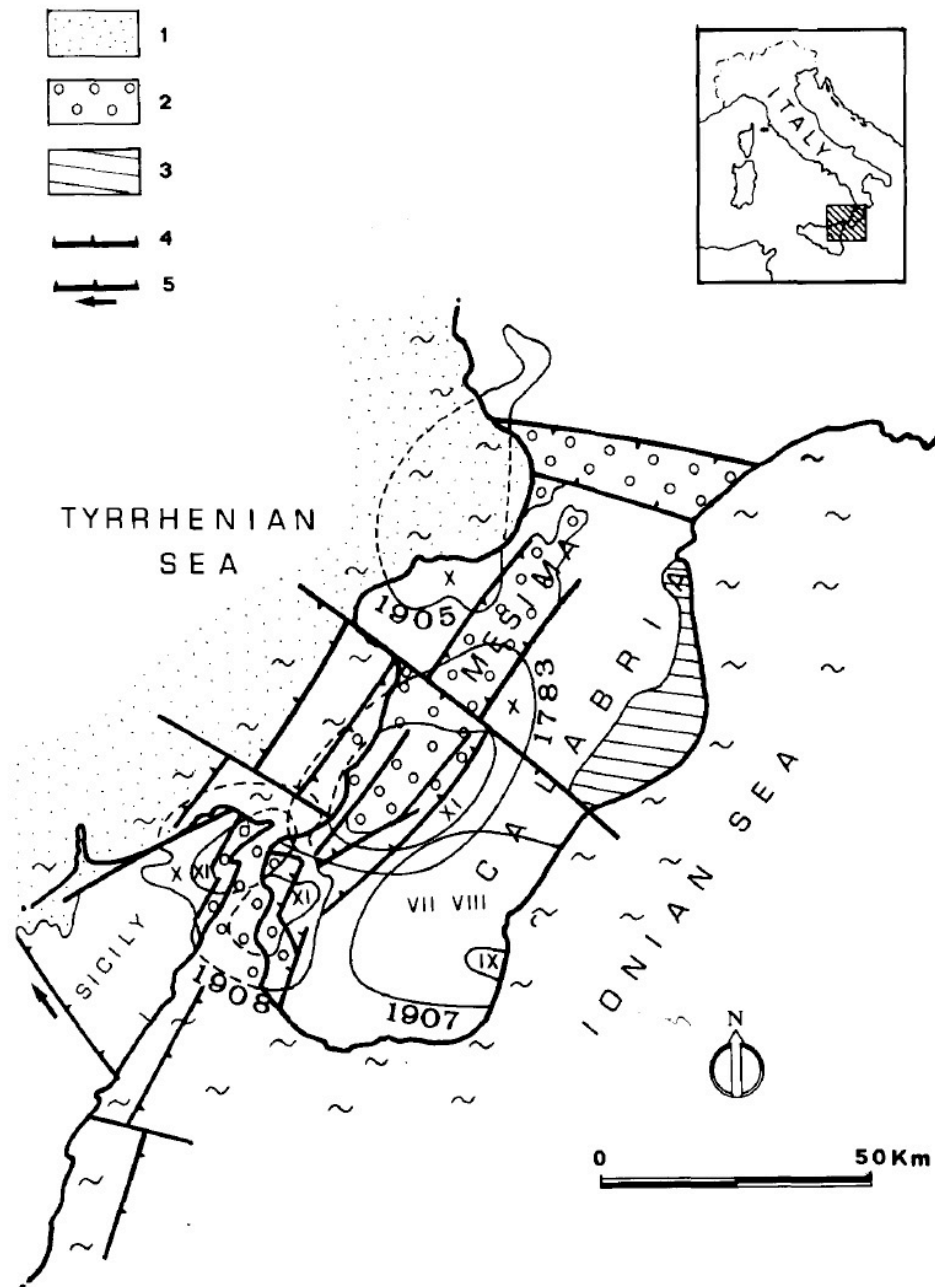
FIG. 2. Schematic seismotectonic map of the Calabrian arc and intensity distribution during the 1908 earthquake and some large events in the region. 1 = foundered peri-Tyrrhenian basin and downfaulted peri-Tyrrhenian margins; 2 = tectonic throughs opened within the axial part of the chain; 3 = external Pliocene-Pleistocene basins; 4 = main systems of normal faults; 5 = fault systems offsets in Middle Pliocene times, and normal activity in Pleistocene times.
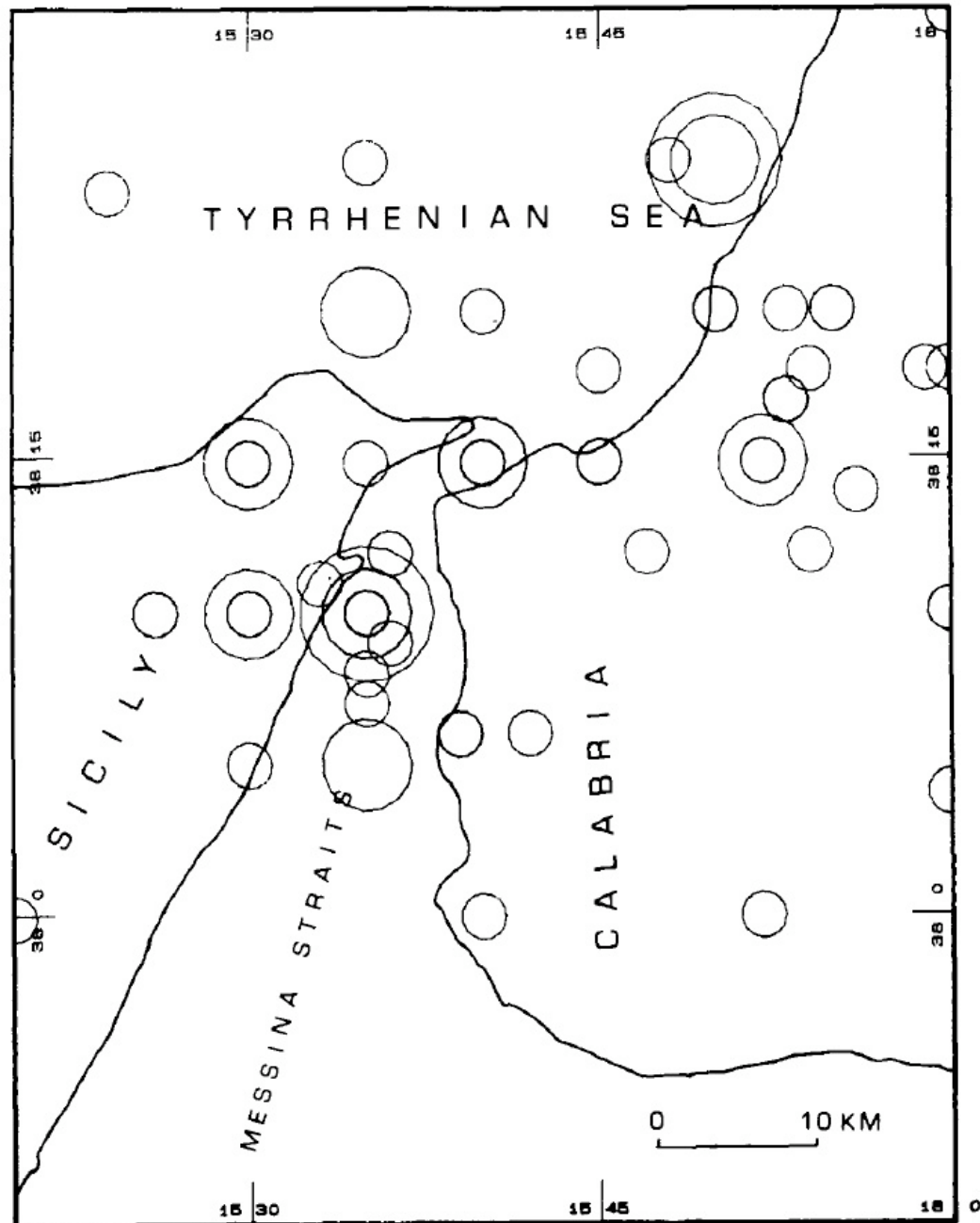
FIG. 3. Earthquakes with $M_l > 4$ occurred in the period 1000 A.D. to 1981 A.D. Radii of the circles are proportional to the event magnitude and are divided in three classes: $4 < M_l \leq 5$, $5 < M_l \leq 6$, $M_l > 6$.
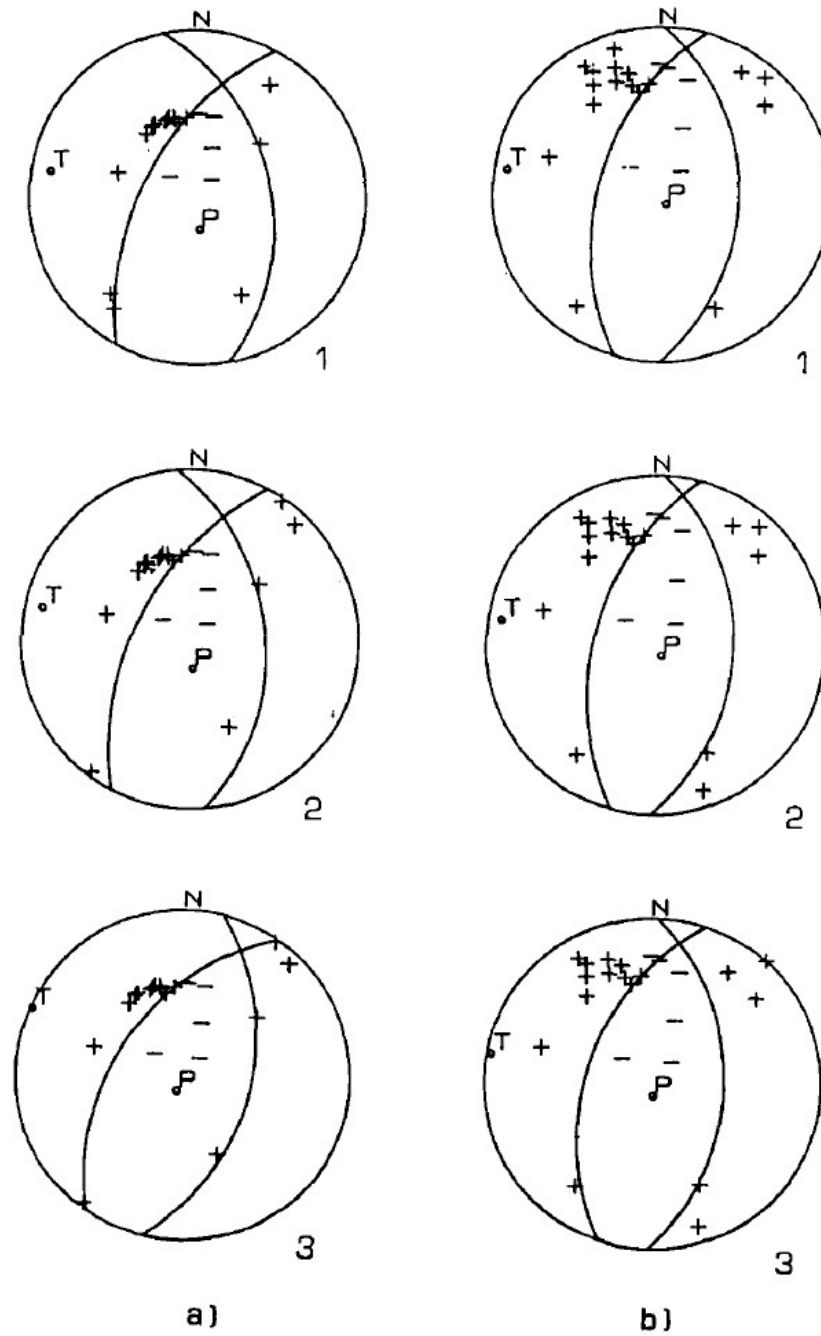
Capuano et al 1988

FIG. 4. Focal mechanism of the 1908 earthquake as inferred by *P*-wave polarities using different velocity models and depth location; a) velocity model by Herrin *et al.*, 1968; b) velocity model by Jeffreys-Bullen, 1967. 1—depth = 10 km; 2—depth = 15 km; 3—depth = 20 km.
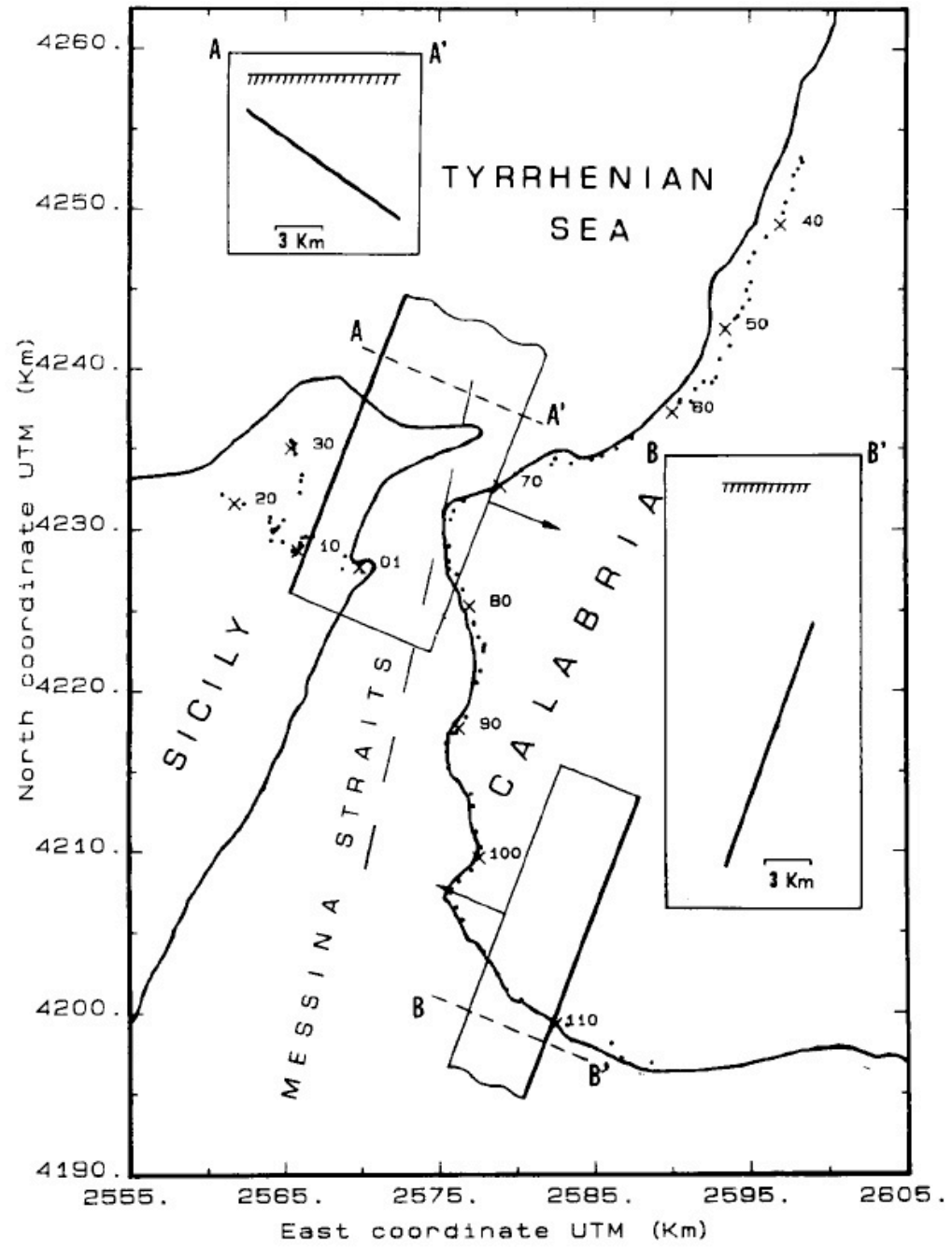
Capuano et al 1988

FIG. 5. Faulting model proposed by Schick (1977) (broken line) and graben model by Mulargia and Boschi (1983) (solid lines). Arrows indicate the slip direction on the upper side of the fault plane; length is proportional to dislocation in arbitrary units.
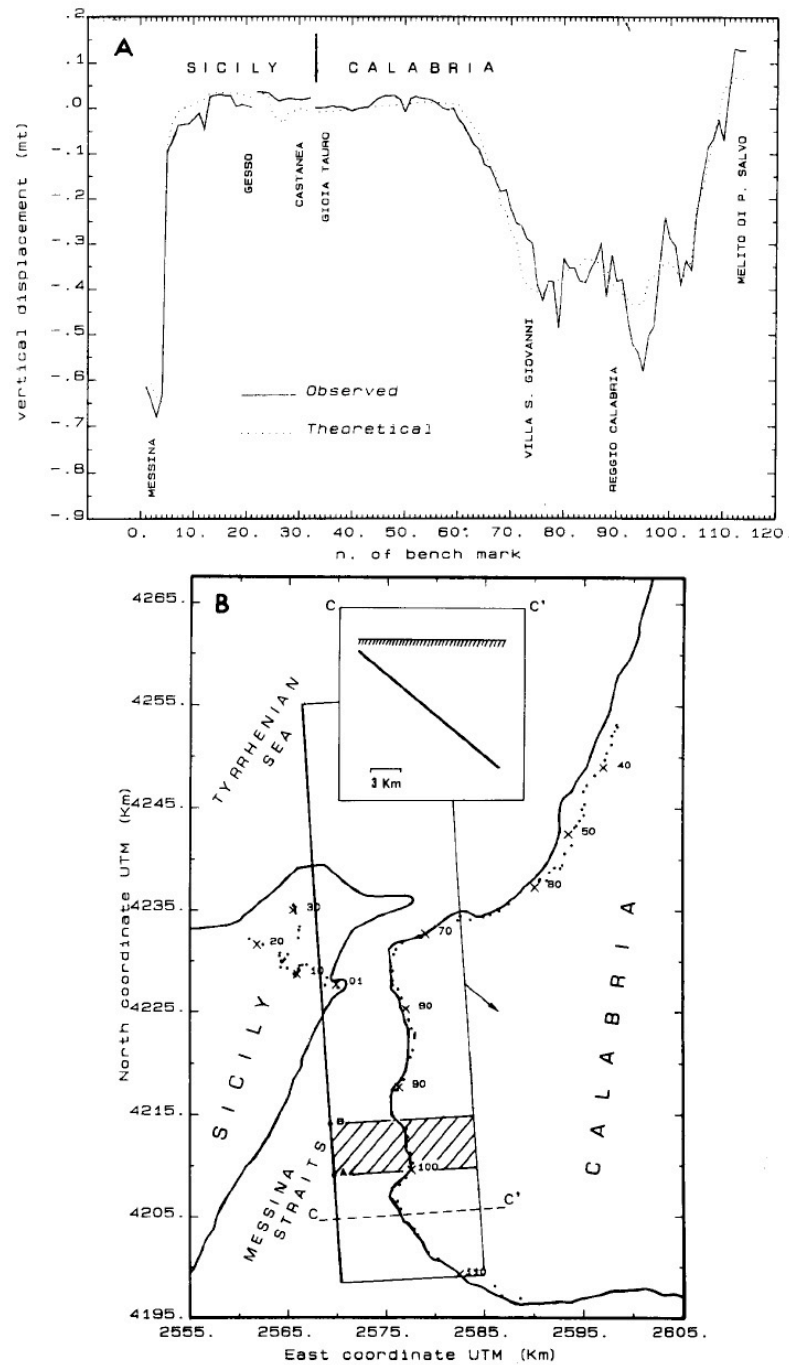
Capuano et al 1988

Capuano et al 1988

FIG. 6. (a) Comparison between observed and theoretical vertical displacement, with a single fault model; (b) surface projection of the fault. Arrow as in Figure 5.
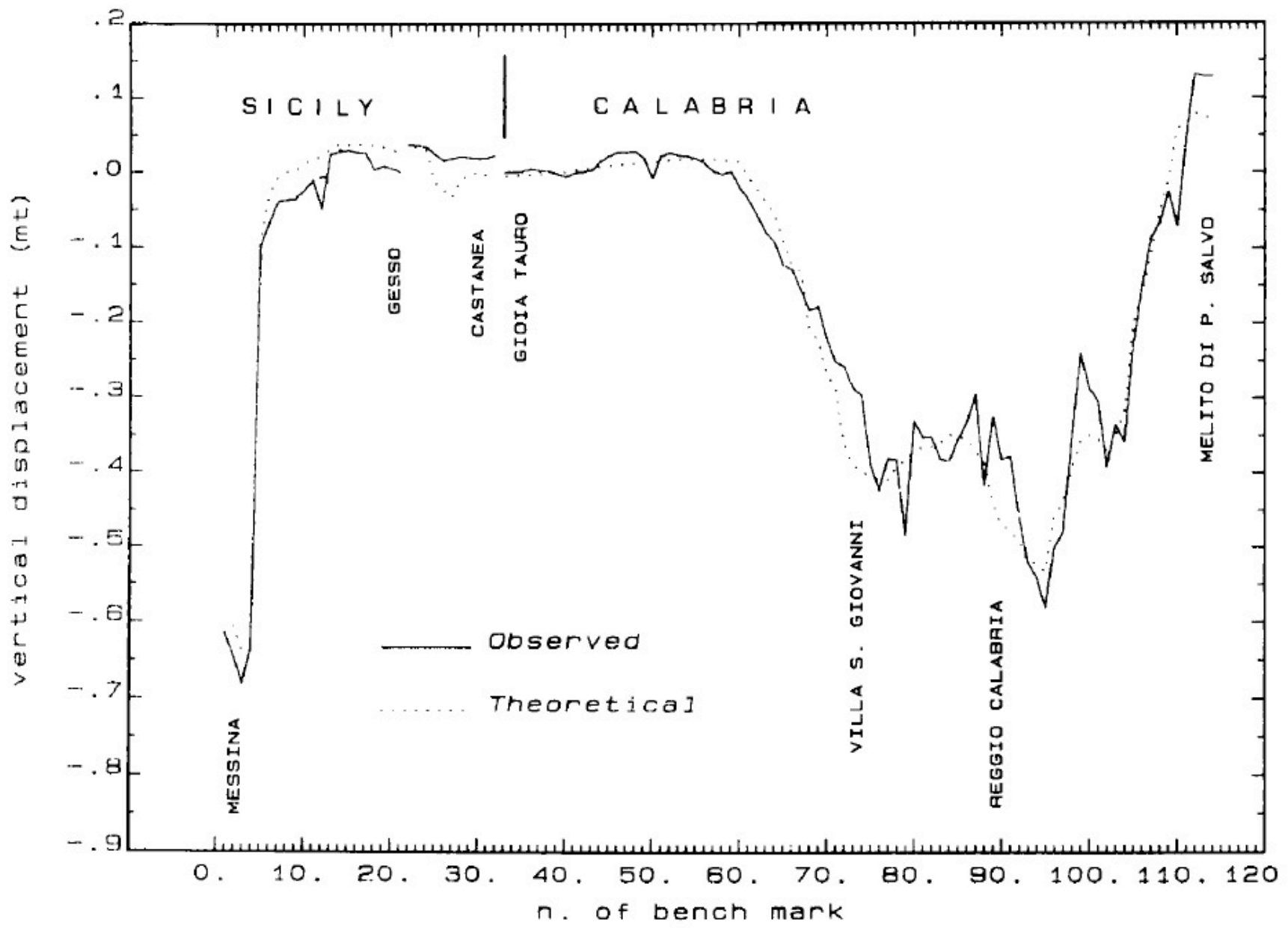
FIG. 7. Comparison between observed and theoretical displacements derived from a model with a stronger dislocation on patch A–B of the fault shown in Figure 6b.
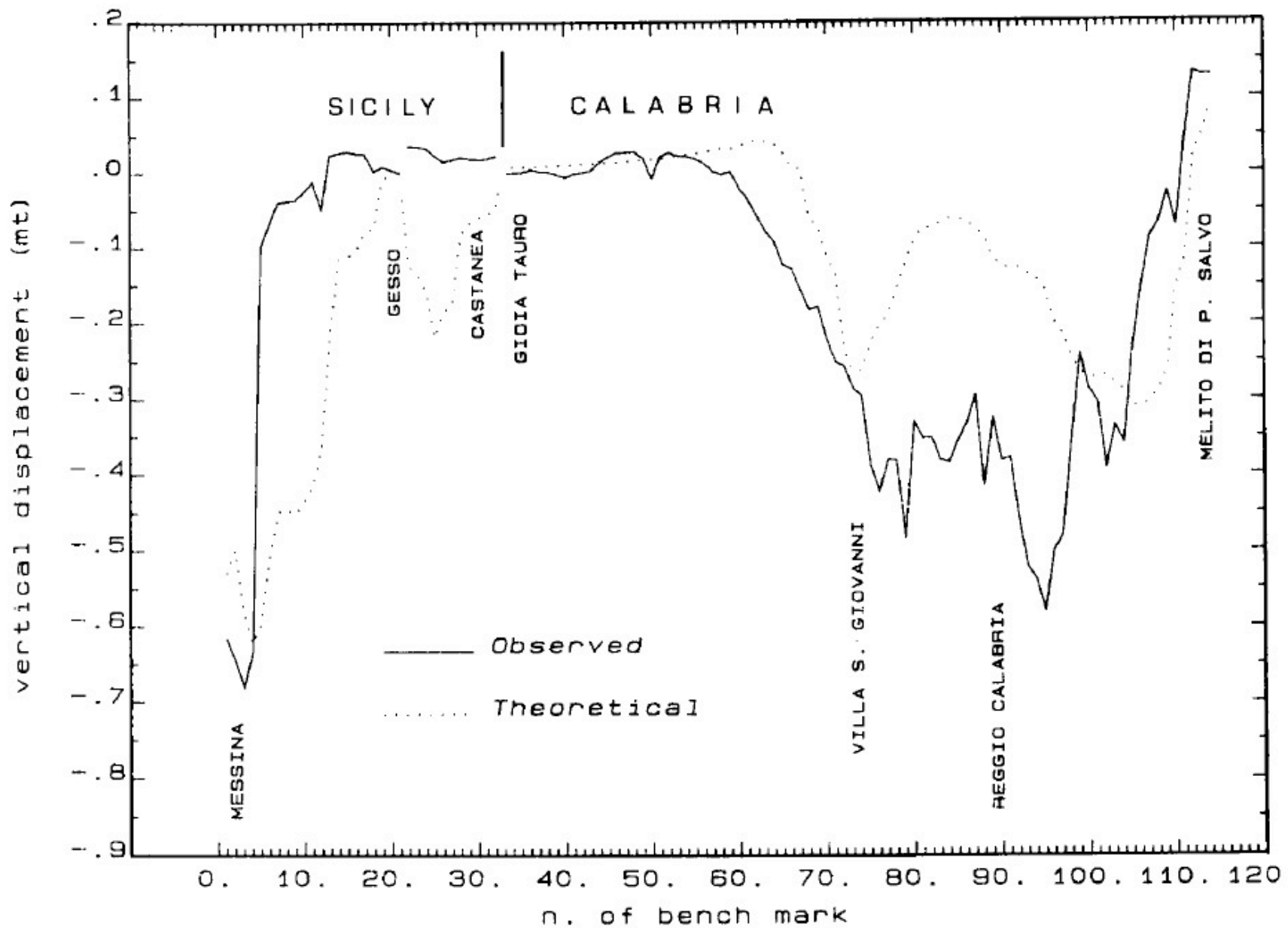
Capuano et al 1988

FIG. 8. Comparison between observed and theoretical displacements derived from the initial two-fault model.
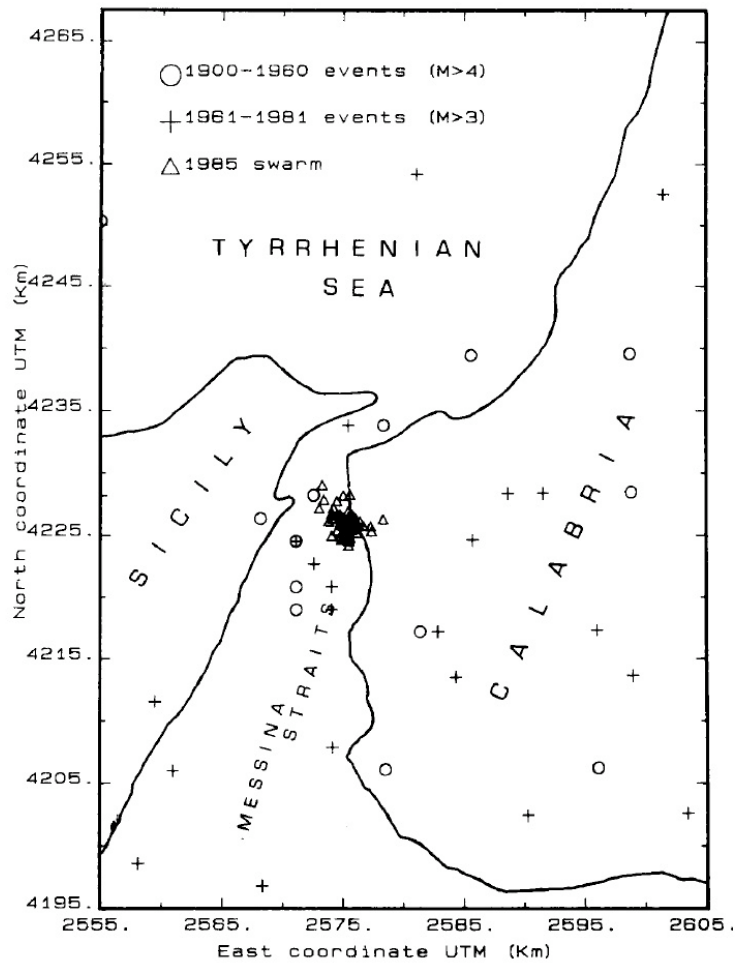
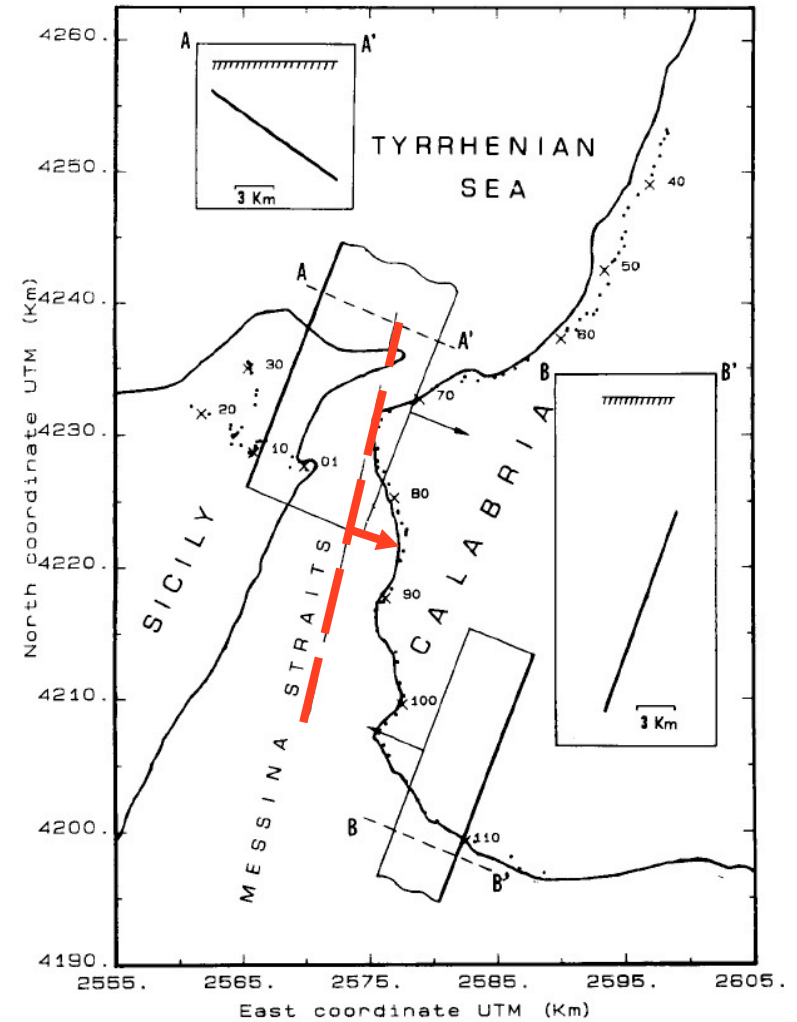FIG. 10. Seismicity map in the period 1900 to 1985.

FIG. 5. Faulting model proposed by Schick (1977) (broken line) and graben model by Mulargia and Boschi (1983) (solid lines). Arrows indicate the slip direction on the upper side of the fault plane; length is proportional to dislocation in arbitrary units.

Capuano et al 1988

**Fig. 1 a** Schematic tectonic framework of Italy. **b** Seismicity of the Northern Apennines (after Boccaletti et al. 2004)
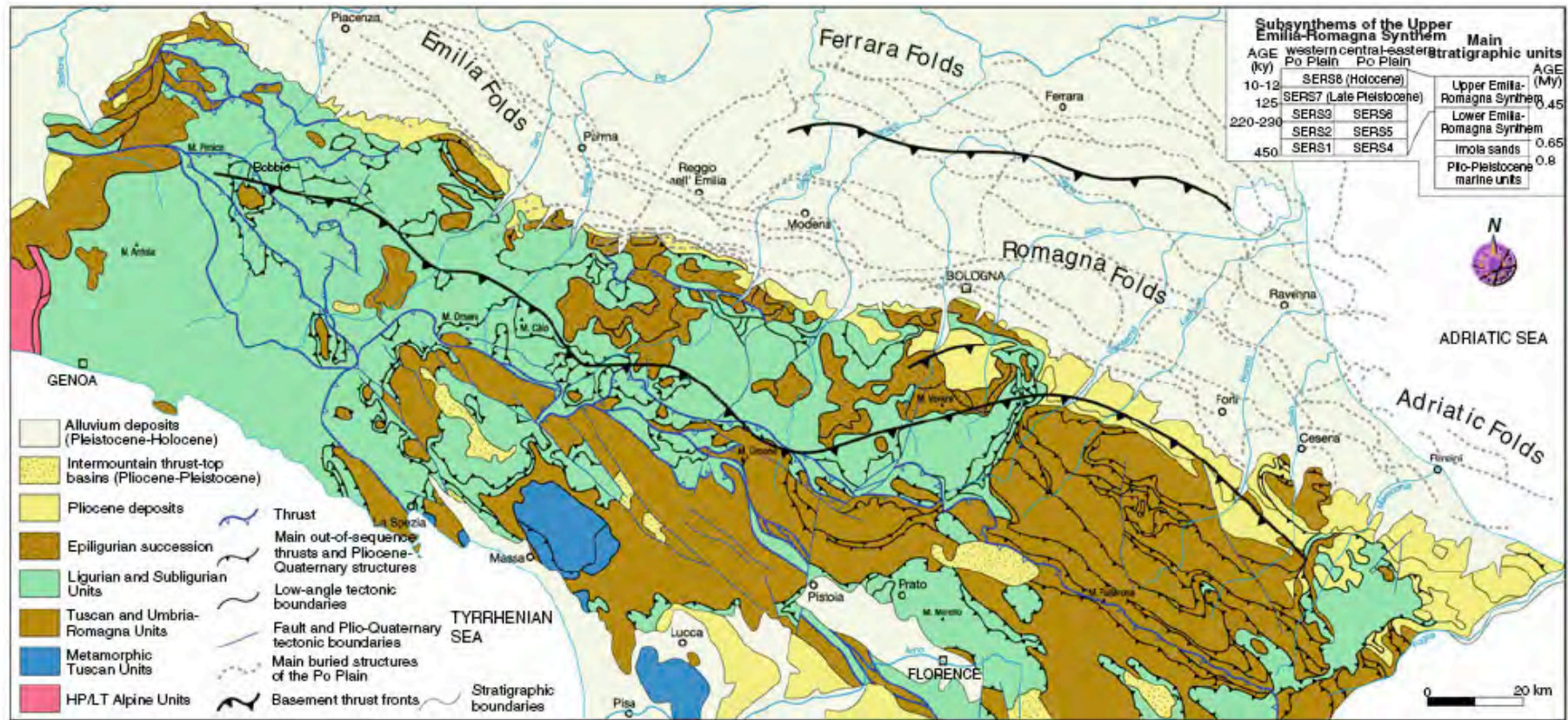
Boccaletti et al 2011
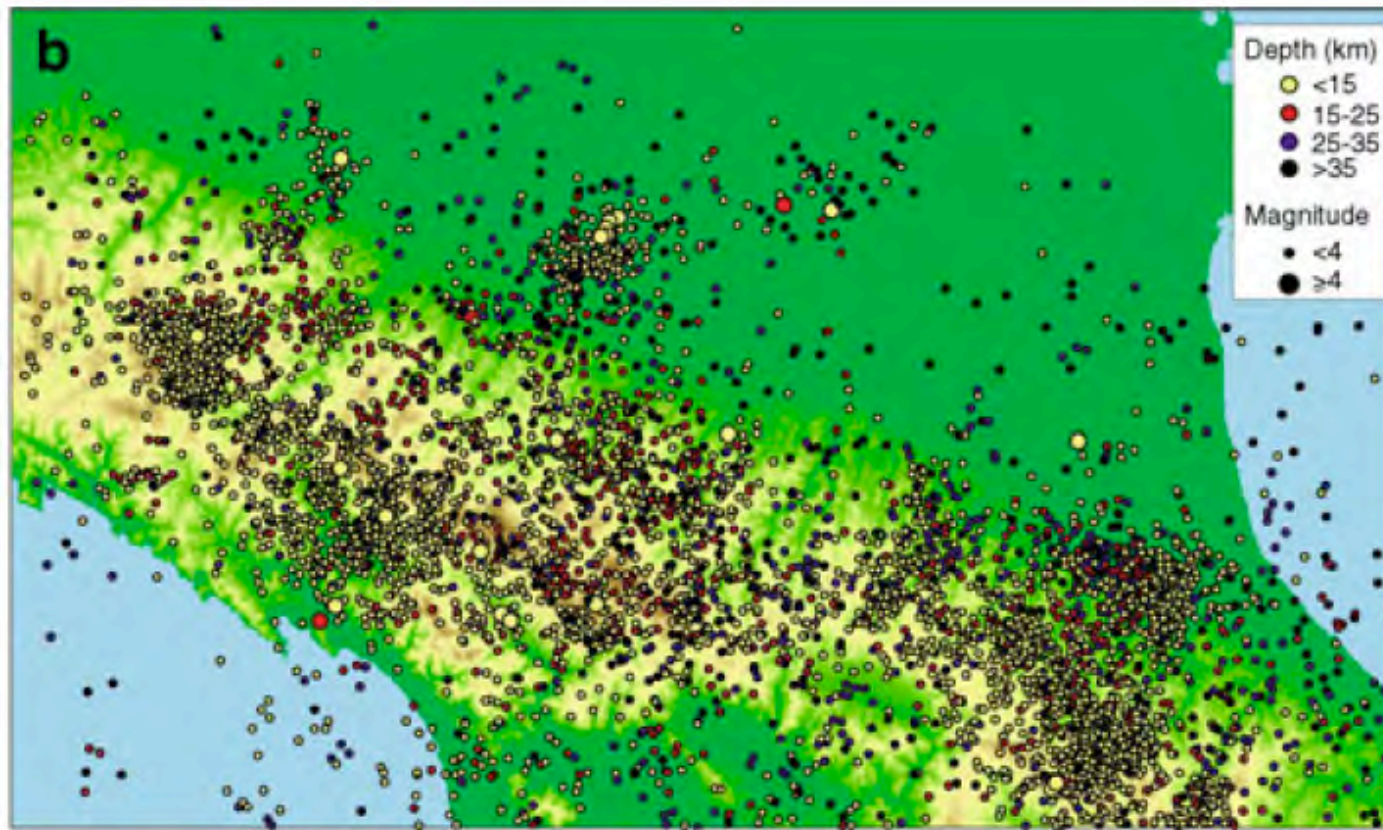
**Fig. 2** Tectonic scheme of the Northern Apennines (after Pieri and Groppi 1981; Cerrina Feroni et al. 2002). *Inset on right upper corner* shows a stratigraphic scheme of the Neogene-Quaternary units of the Po Plain and the Apennines–Po Plain margin
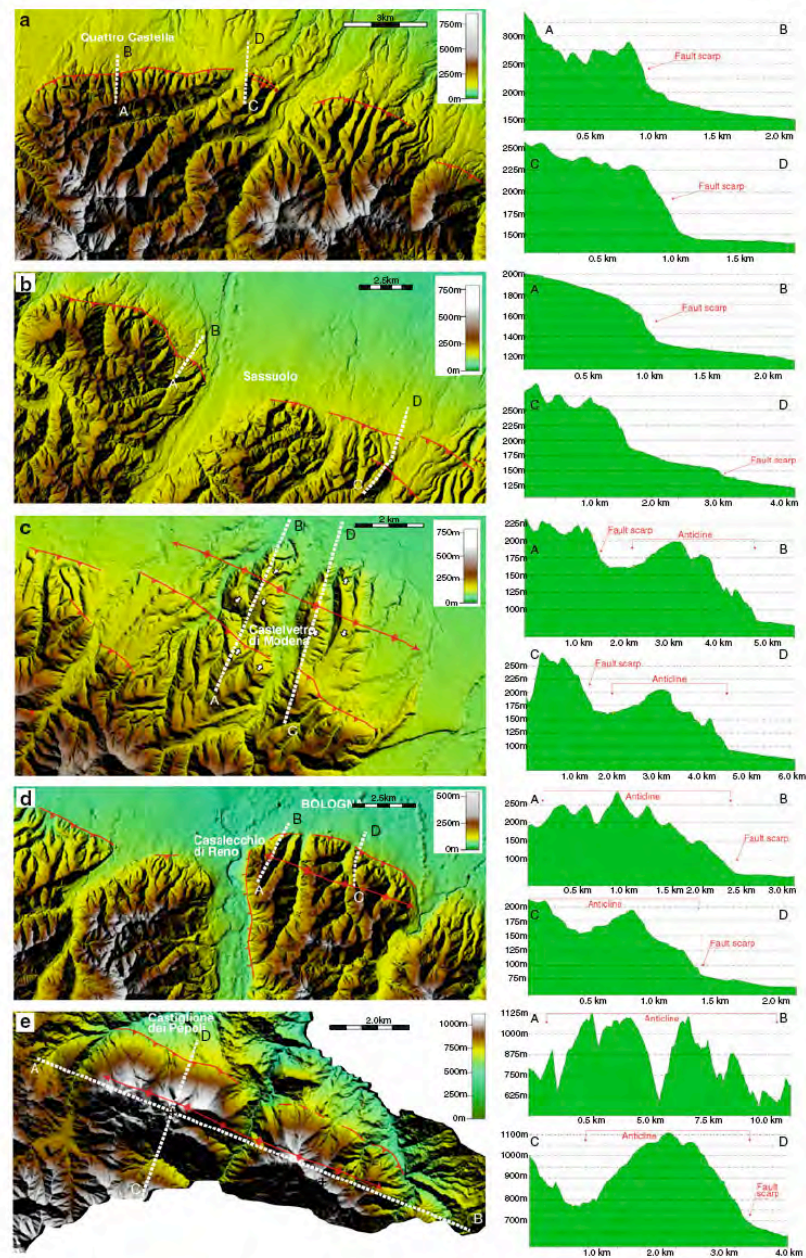
Boccaletti et al 2011

Fig. 4 Details of recent and active structures in the external part of the Northern Apennines illustrated as digital elevation models (DEMs) with 10-m resolution (*left panels*) and topographic profiles of the main structures (*right panels*). *Insets on left panels* represent a structural sketch of the main structures. **a** Pede-Apenninic Thrust Front near Quattro Castella. Note the prominent fault scarp associated with typical morphostructural features (such as triangular facets). **b** Pede-Apenninic Thrust Front near Sassuolo. **c** Pede-Apenninic Thrust Front and associated growing anticline in the Castelvetro di Modena area. *Arrows* indicate the tilting direction of paleo-surfaces. **d** Pede-Apenninic Thrust Front and associated growing anticline in the Bologna area. **e** Castiglione dei Pepoli thrust front and growing anticline. Location of different panels is reported in Fig. 3
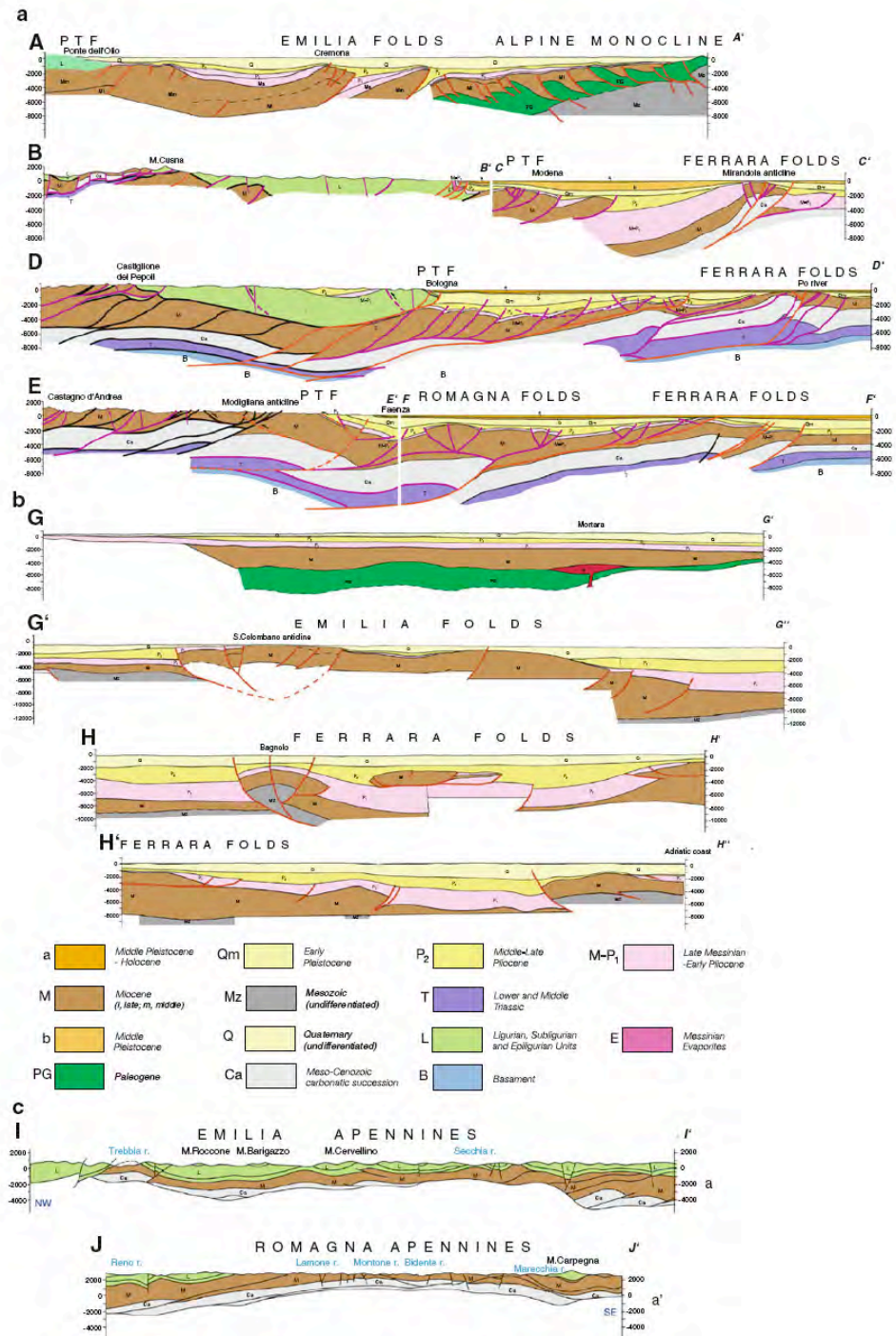
**Fig. 6** **a** Alluvial terraces (<220,000 year) in the S. Sofia area (Bidente valley); **b** tilted alluvial deposits (Lower Emilia-Romagna Synthem, 0.65–0.45 M year) (Tiepido valley, Modena Apennines–Po Plain margin); **c** overturned Imola Sands (0.8–0.65 M year) (Reno valley, Bologna Apennines–Po Plain margin); **d** Thrust faults affecting the Imola Sands (0.8–0.65 M year) (Panaro valley, Modena Apennines–Po Plain margin)
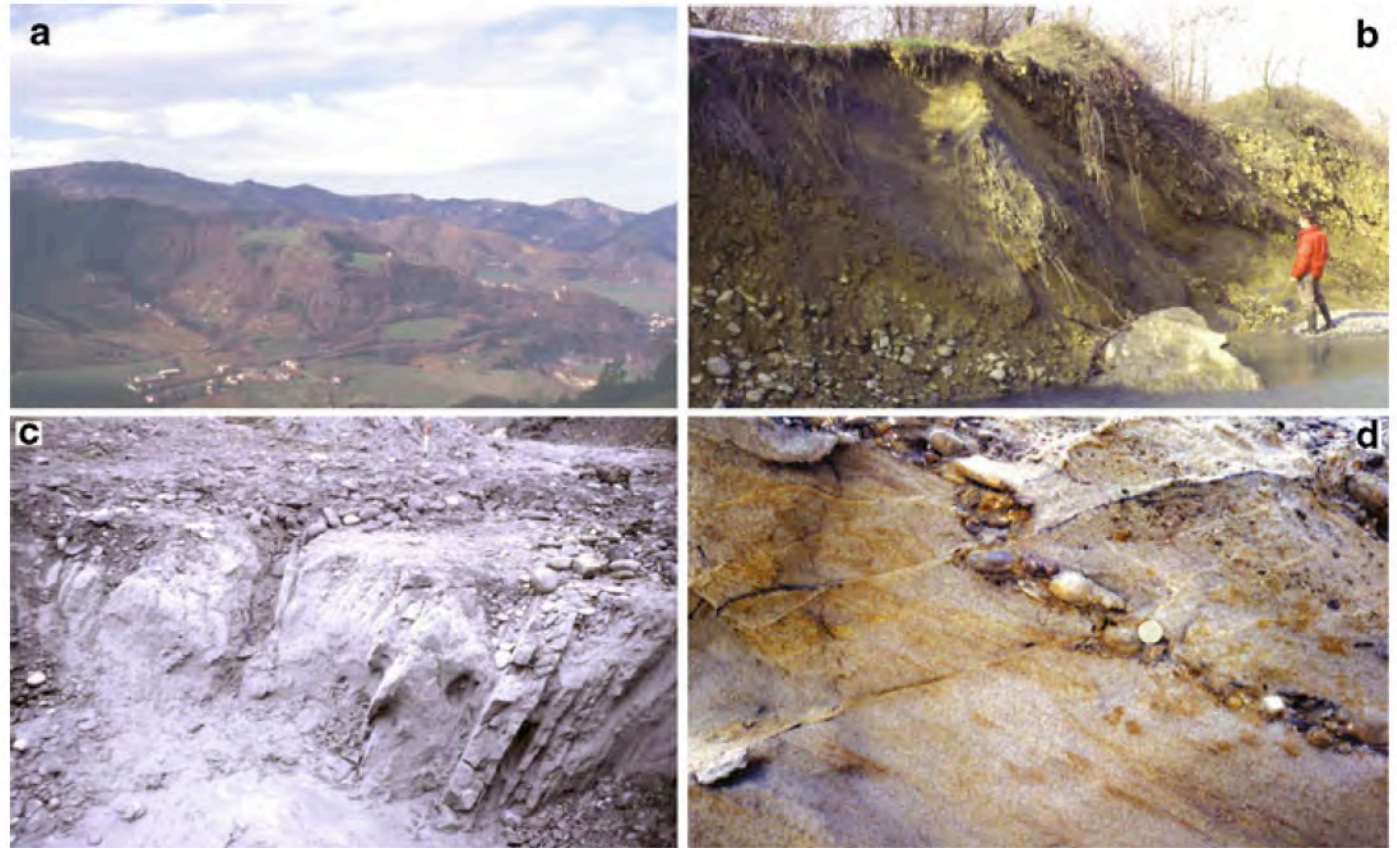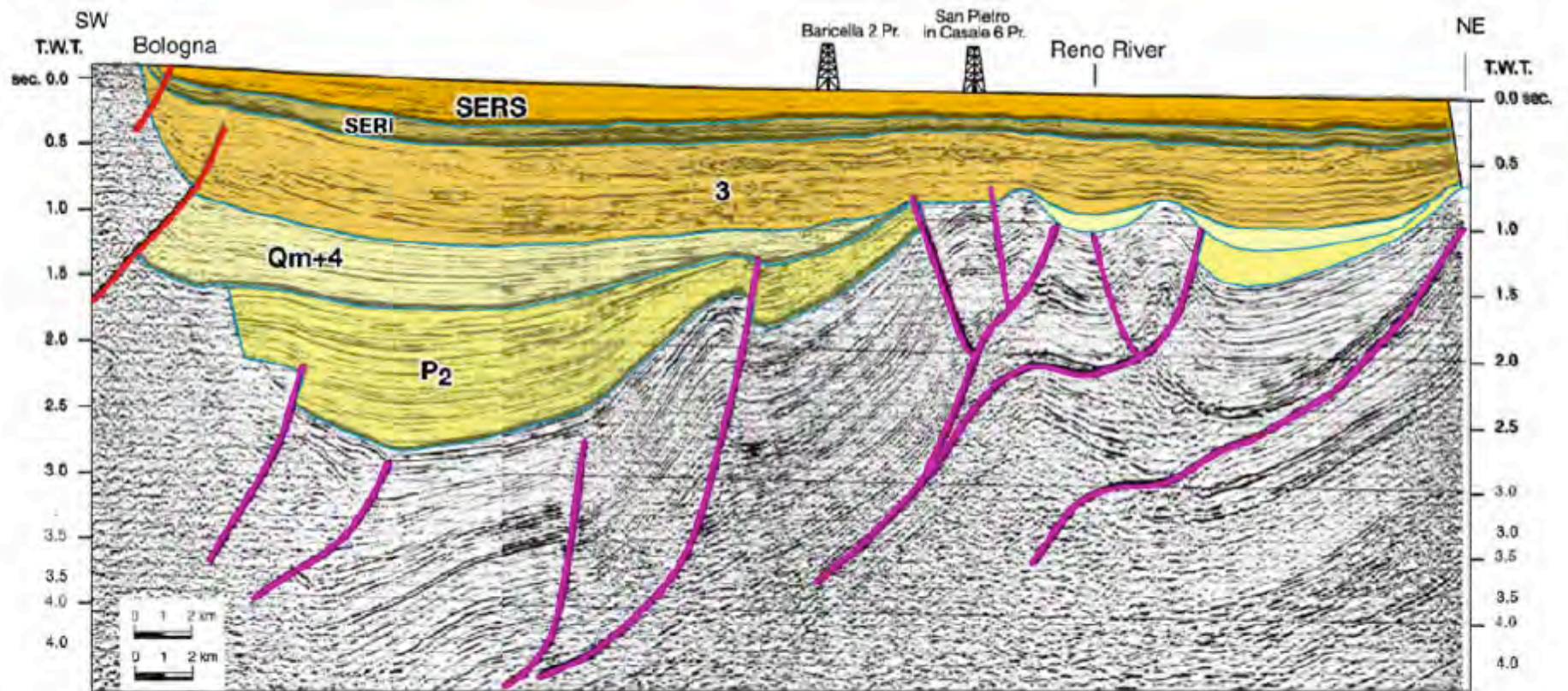
Fig. 7 Example of interpreted seismic line (modified from RER and ENI-Agip 1998). Note that Middle Pleistocene and Late Pleistocene units (3: Imola Sands; SERI: Lower Emilia-Romagna Synthem; SERS: Upper Emilia-Romagna Synthem) are folded and faulted. P2: Late Pliocene; Qm: Lower Pleistocene marine sediments; 4: Yellow Sands (1–0.8 M year)
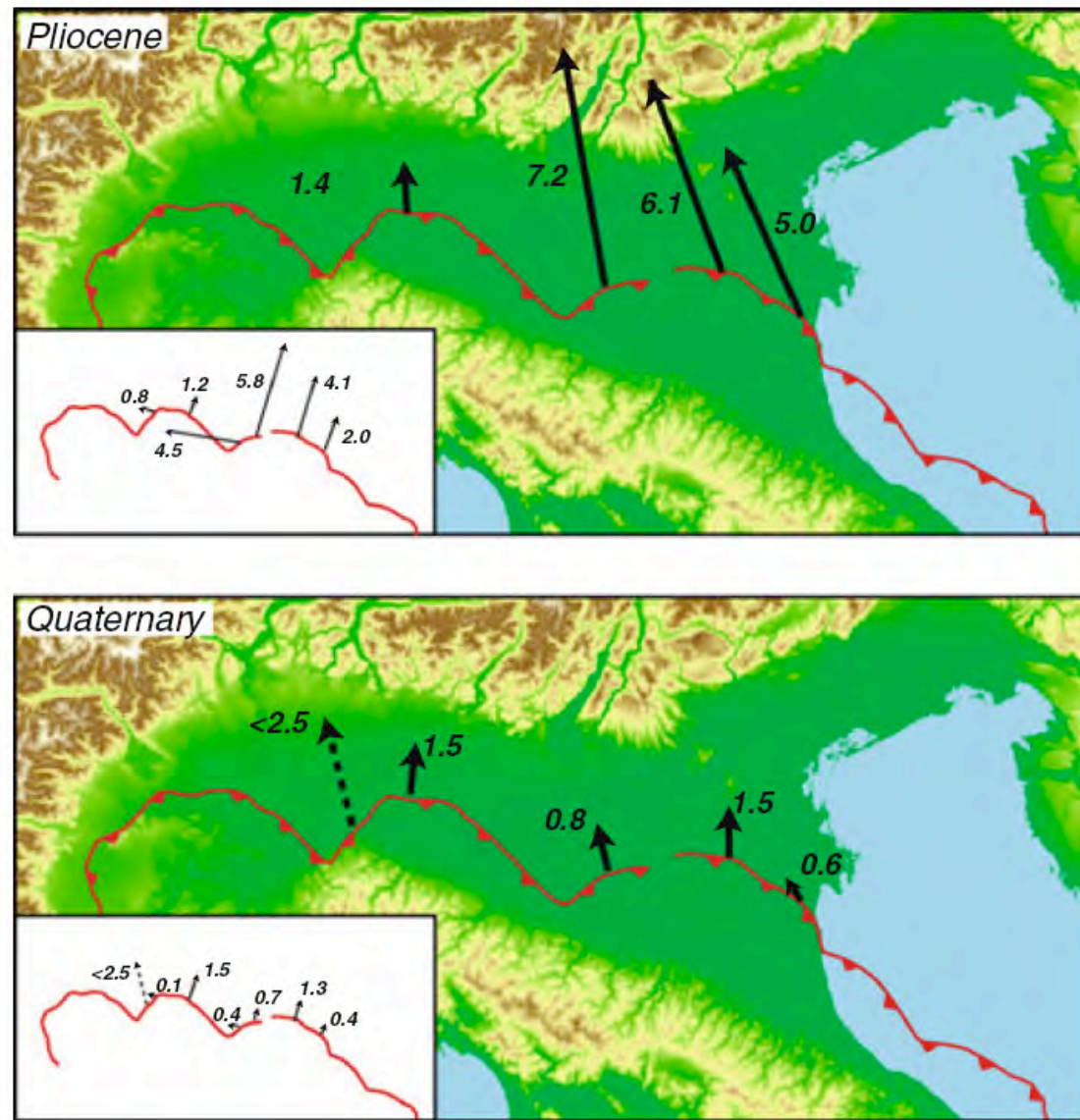
Boccaletti et al 2011

**Fig. 10** Pliocene and Quaternary slip rates calculated from the main structures from analysis of available seismic sections. *Inset* shows rates along WNW–ESE and NNE–SSW seismic lines used to calculate the real shortening directions (see "Appendix" for details of calculations)
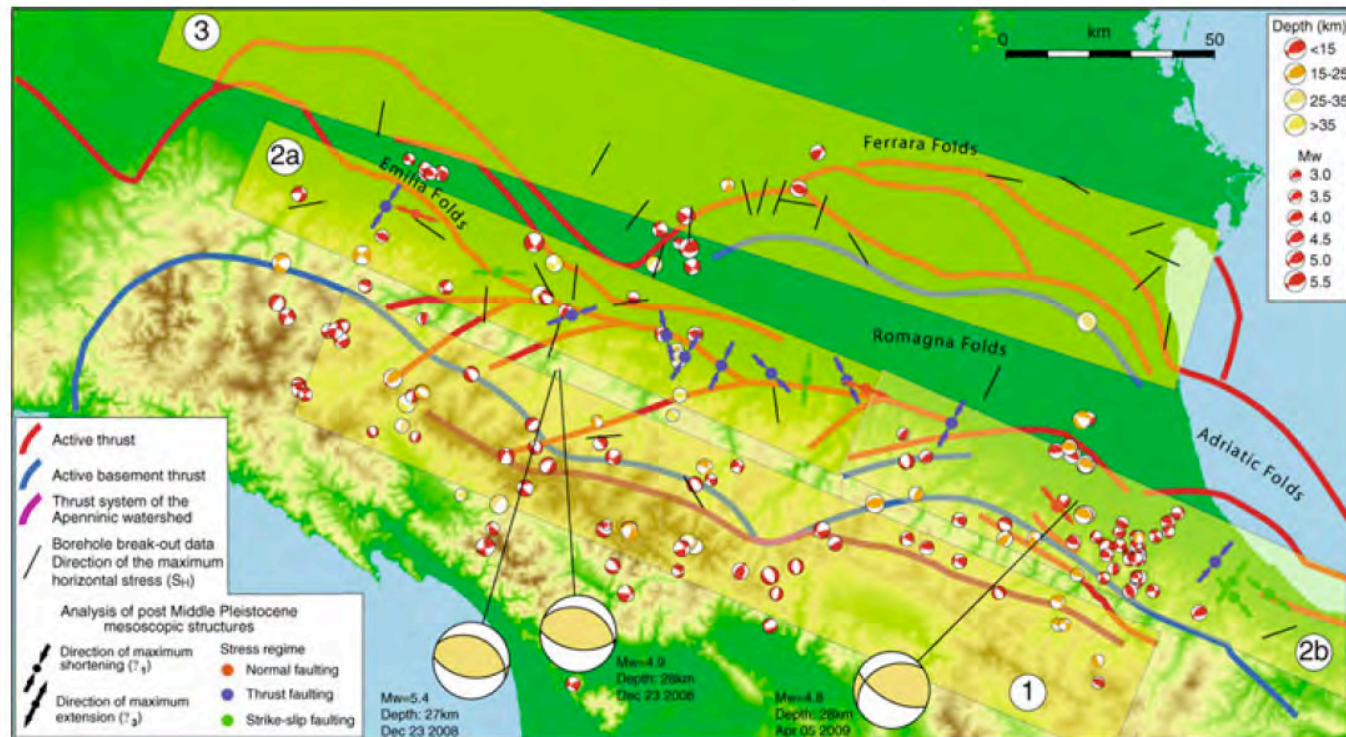
**Fig. 11** Summary of the recent and active structures of the external Northern Apennines with superimposed focal mechanism solutions (Boccaletti et al. 2004), stress fields from mesoscopic analysis (Ghiselli and Martelli 1997) and borehole breakout data (Mariucci and Muller 2003). Enlarged are three focal mechanisms of main events of the seismic sequences that effected the external Apennines on December 23, 2008, and April 5, 2009 (from INGV data, http://www.ingv.it). *Numbers in circles* indicate the main fault systems: (*1*) Apenninic chain; (*2a*) Apennines–Po Plain margin (North-Western sector); (*2b*) Apennines–Po Plain margin (South-Eastern sector); (*3*) buried Emilia and Ferrara Folds
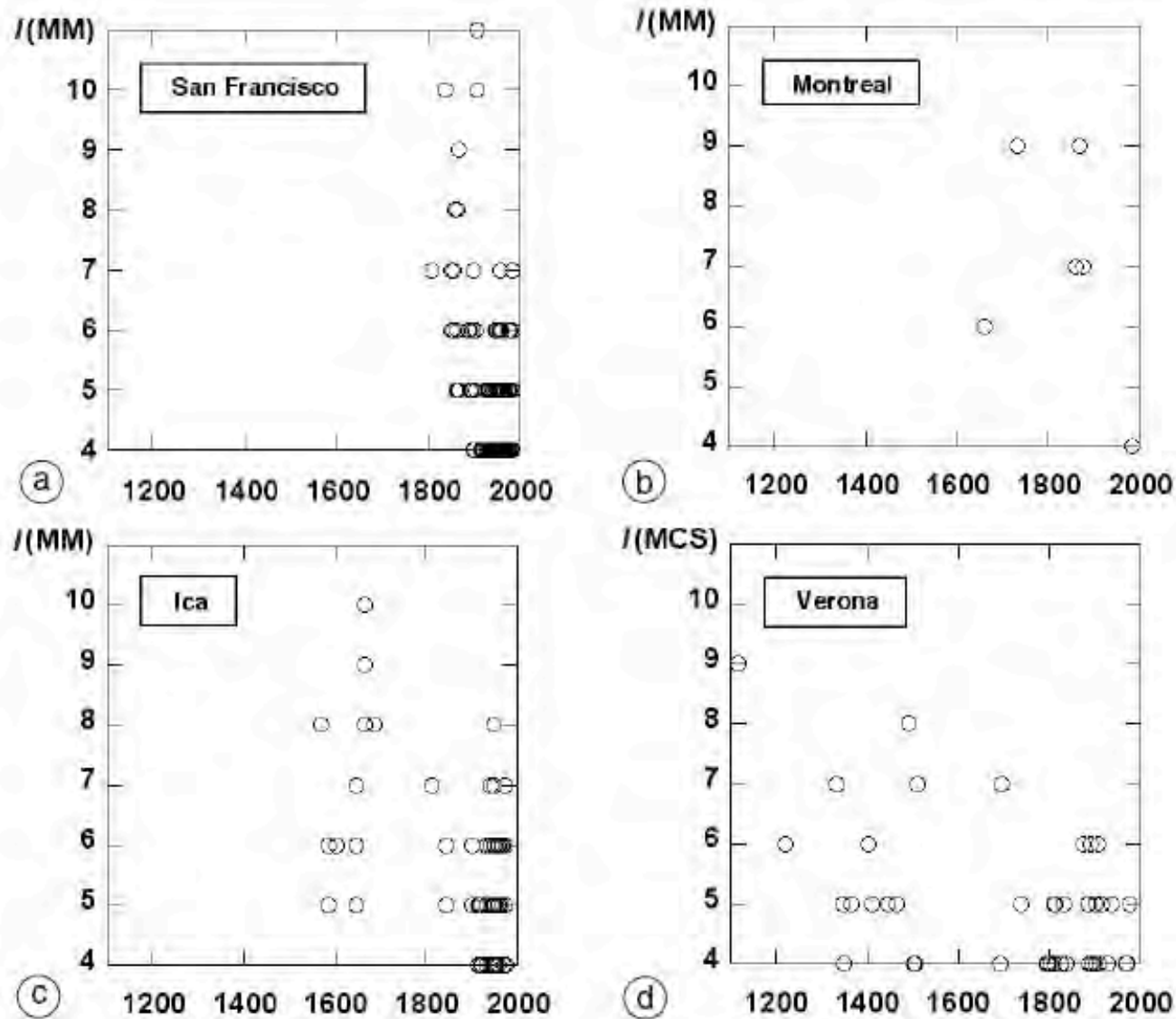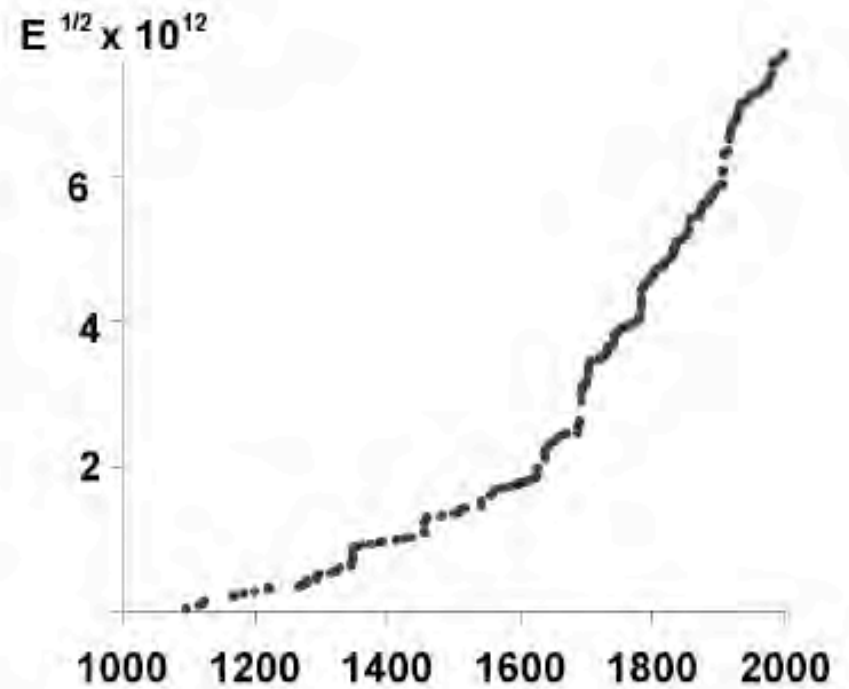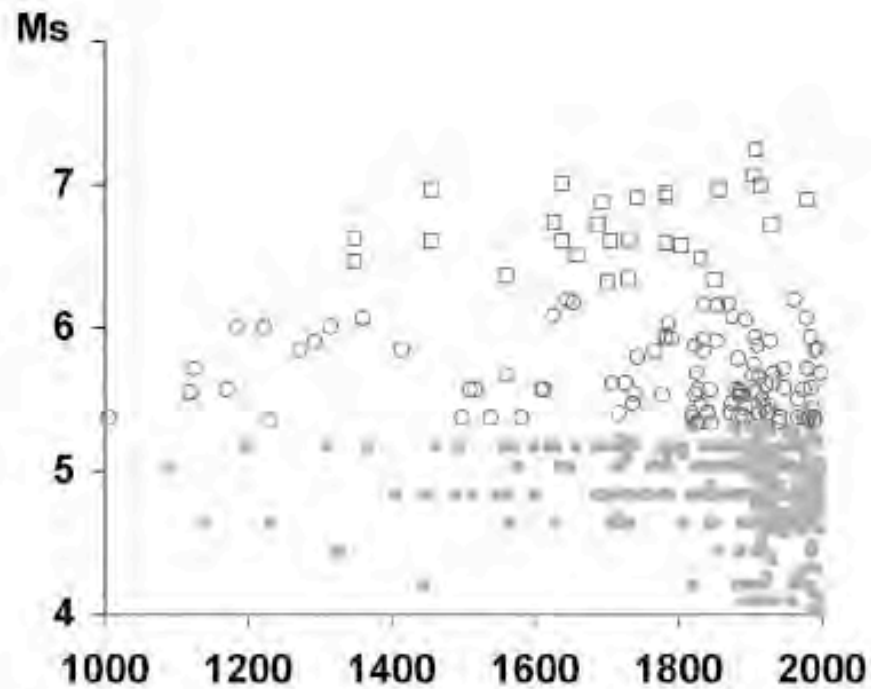
Boccaletti et al 2011

Fig. 1a-d. Seismic histories of (or macroseismic intensities reported at): a) San Francisco, CA, US, b) Montreal, Canada (from US Earthquake Intensity Database, http://www.ngdc.noaa.gov/seg/hazard/eqint.html); c) Ica, Peru (from CERESIS, 1985); d) Verona, Italy (from DOM4.1, Monachesi and Stucchi, 1997).

Stucchi et al 2004

**Fig. 2a,b.** a) Seismic history of Southern Italy; b) cumulative strain release computed for events with $M_s \geq 5.5$ of the Italian CPTI catalogue.
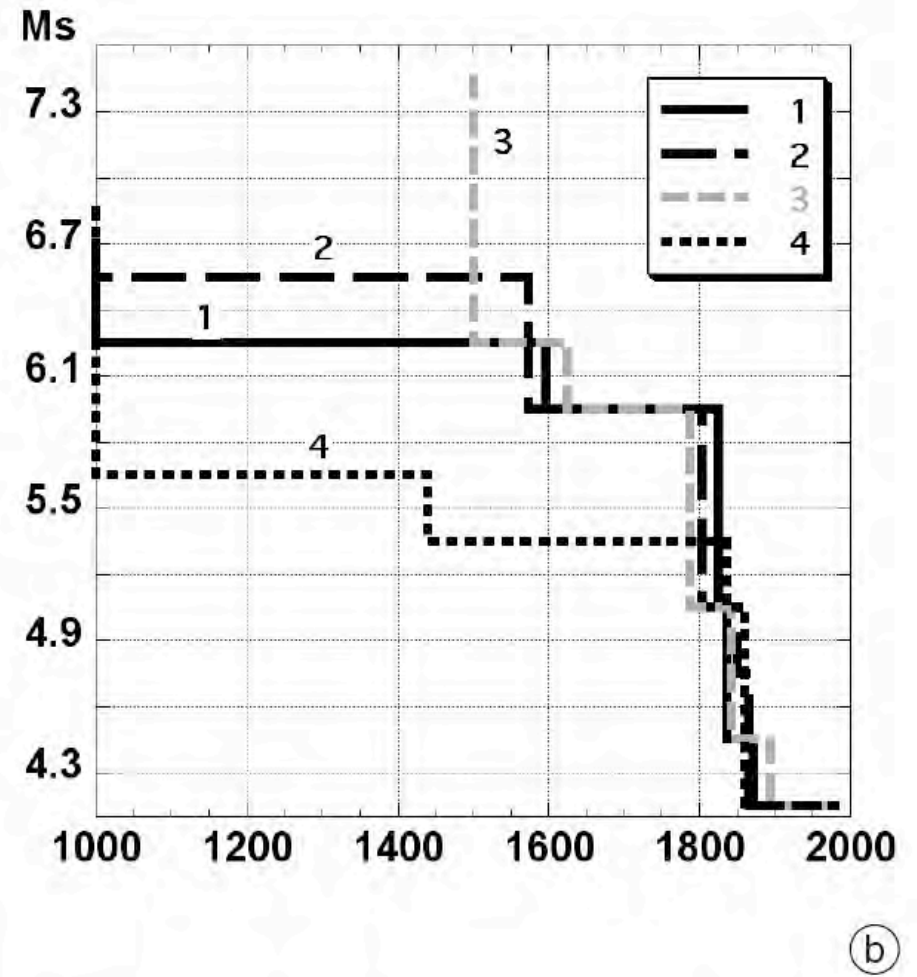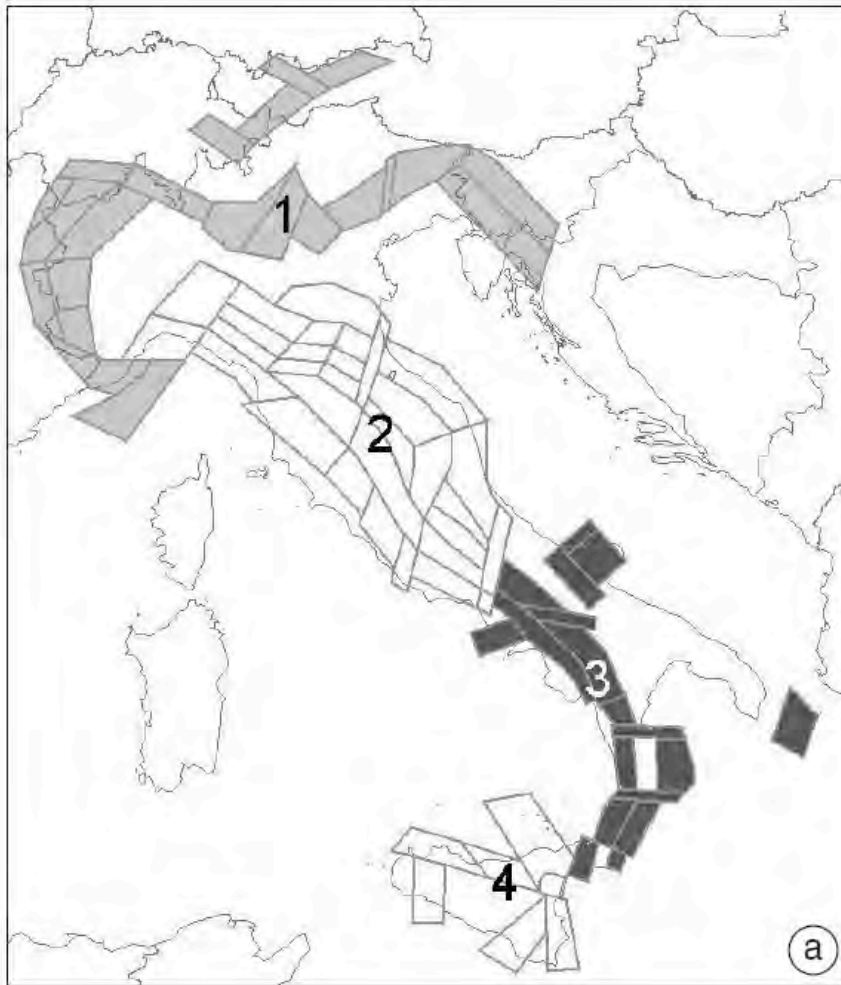
Stucchi et al 2004

**Fig. 4a,b.** a) Homogeneous regions and (b) relevant completeness time-intervals ($M_s$ *versus* time) used by Slejko *et al.* (1998).
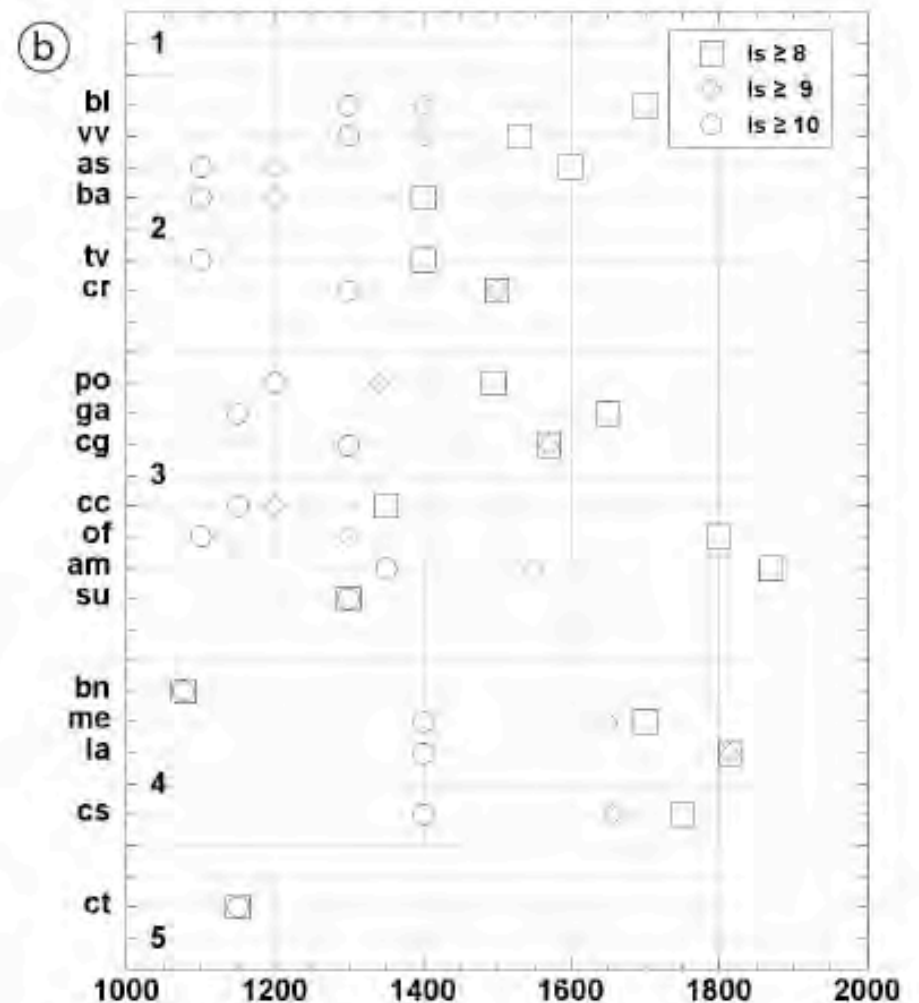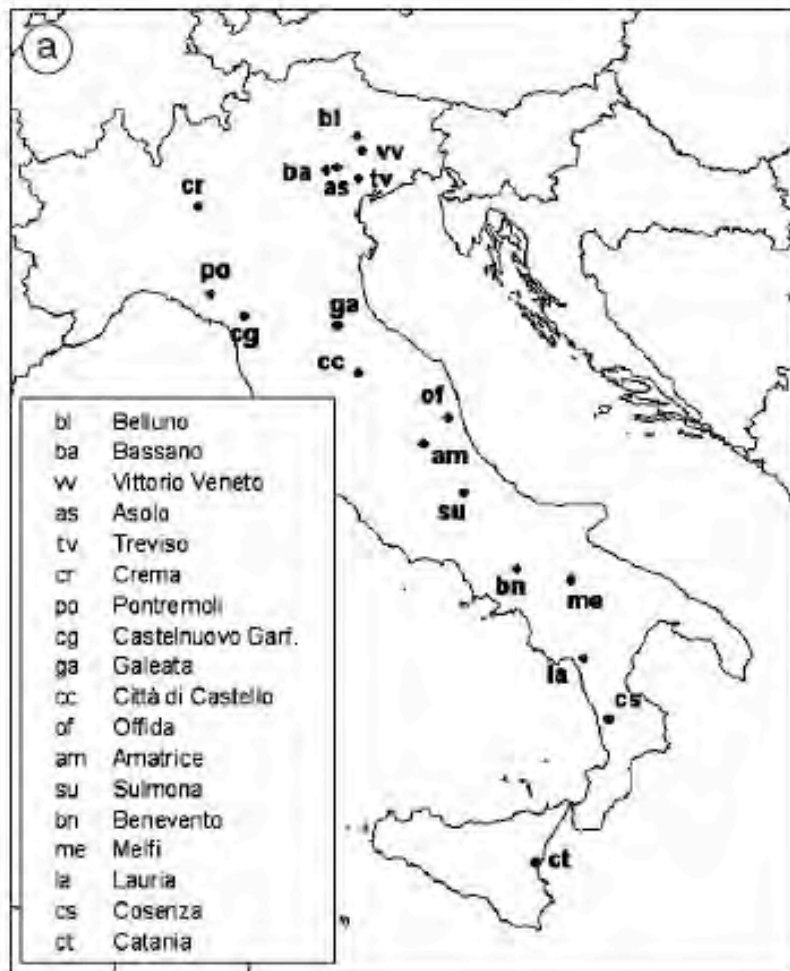
Stucchi et al 2004

**Fig. 6a,b.** a) The 18 localities where the completeness of the site seismic histories was investigated. b) Completeness start times at the investigated localities for site intensity $I_s \geq 8$ MCS (squares), $I_s \geq 9$ MCS (diamonds), $I_s \geq 10$ MCS (circles).
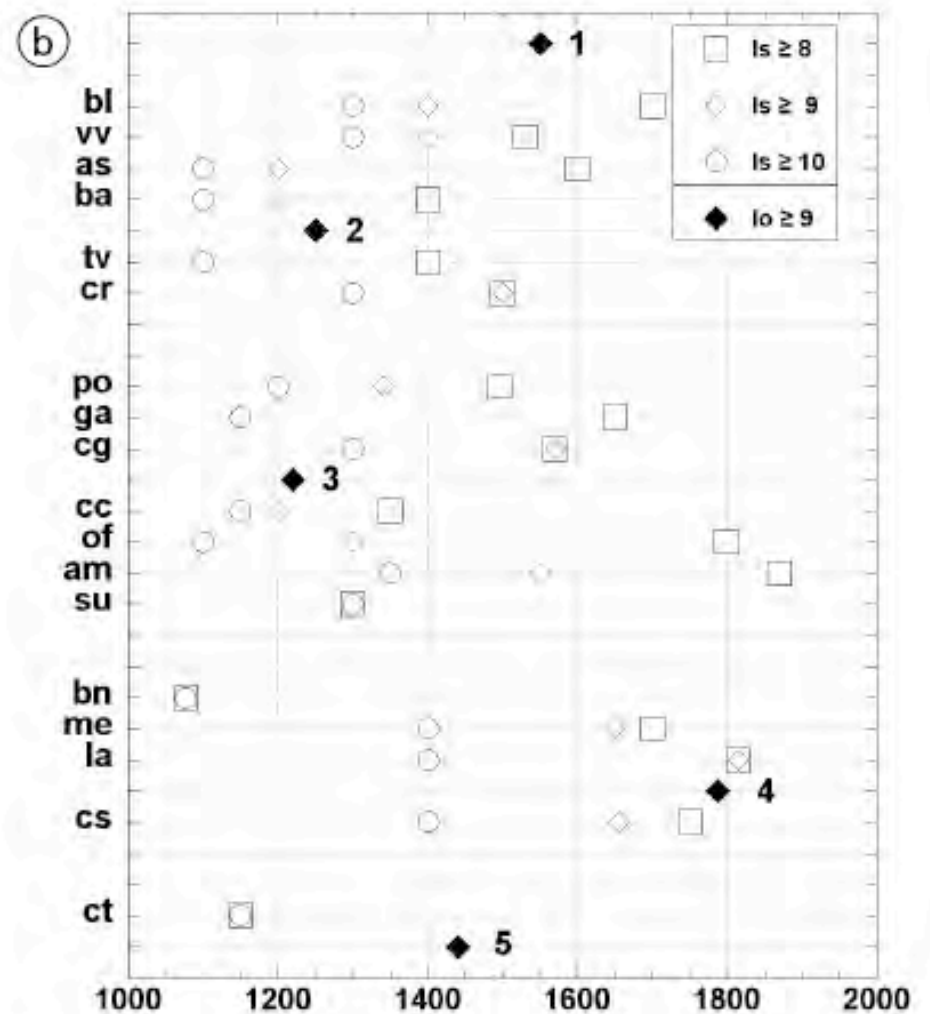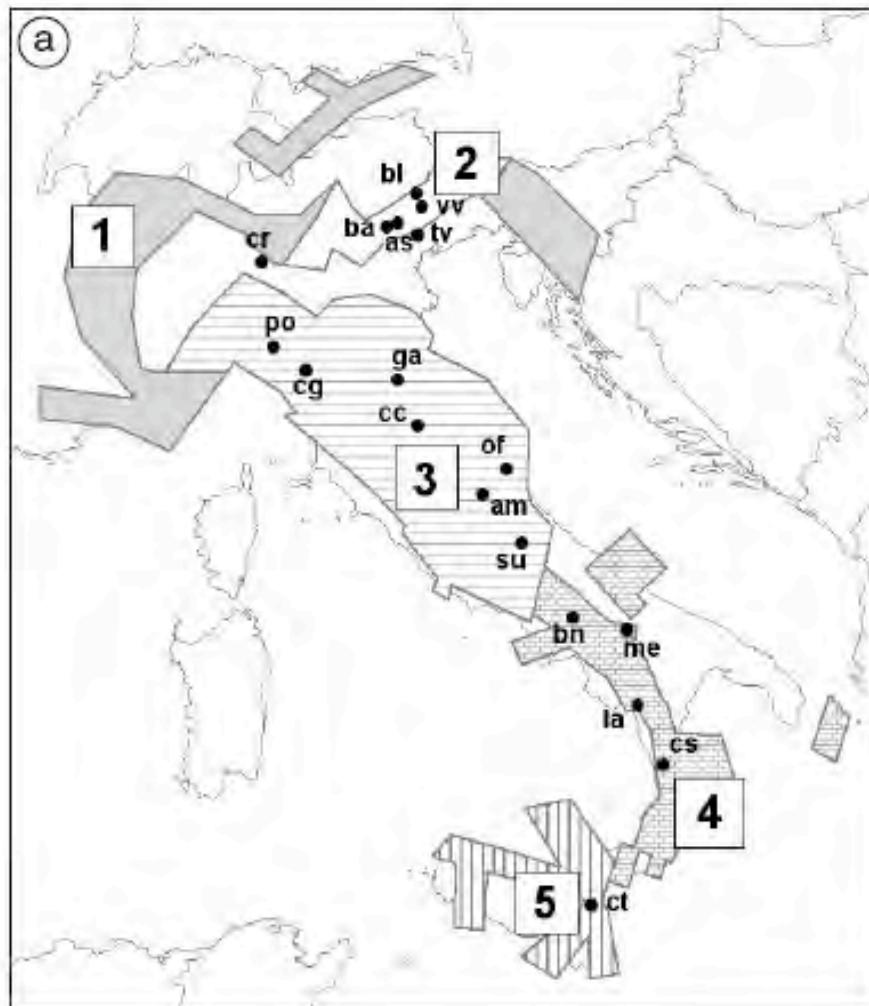
Stucchi et al 2004

**Fig. 7a,b.** a) Homogeneous regions and (b) average relevant completeness start times for $I_0 \geq 9$ MCS or $M_s \geq 6.0$ (full diamonds), superimposed to the data of fig. 6b.
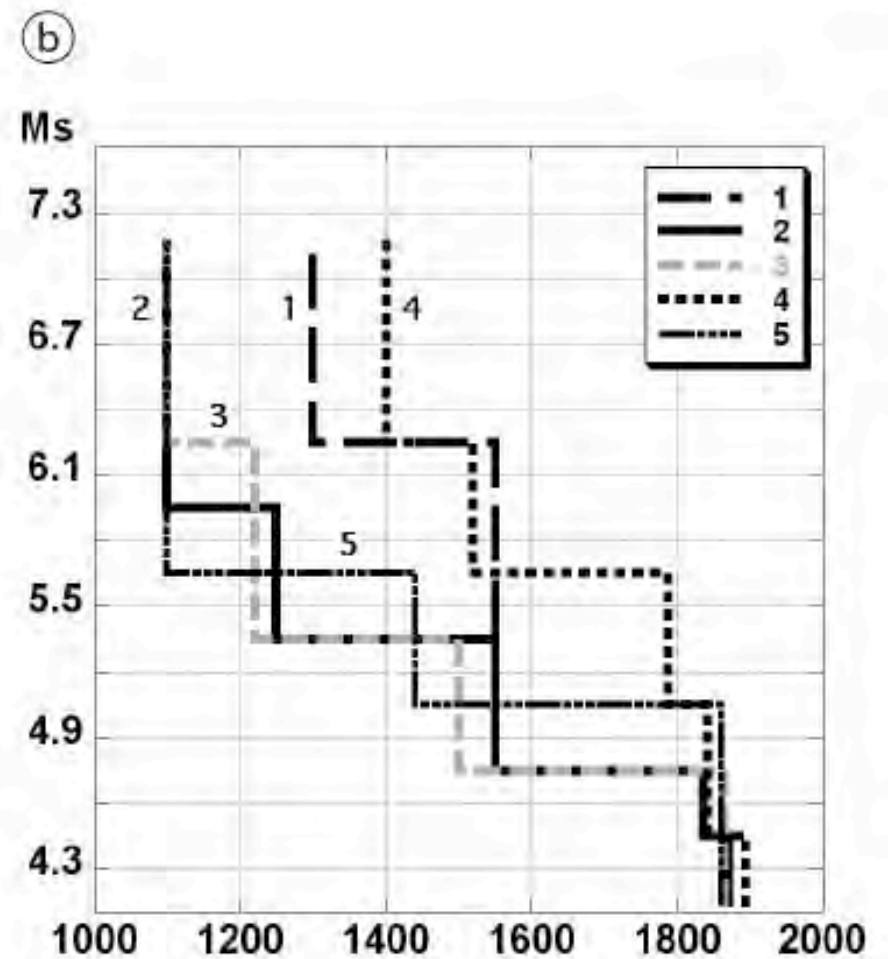
Stucchi et al 2004
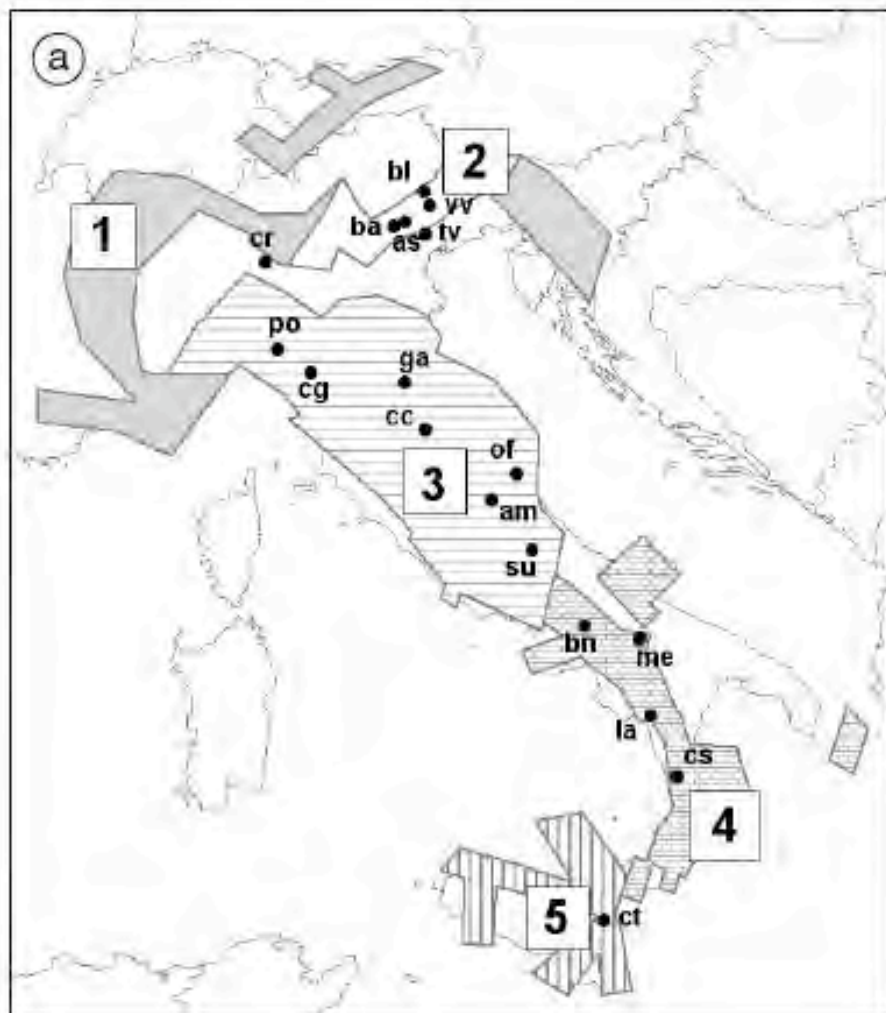
Fig. 8a,b. a) Homogeneous regions; b) broken lines representing the final completeness time-intervals ($M_s$ versus time) in the five regions.
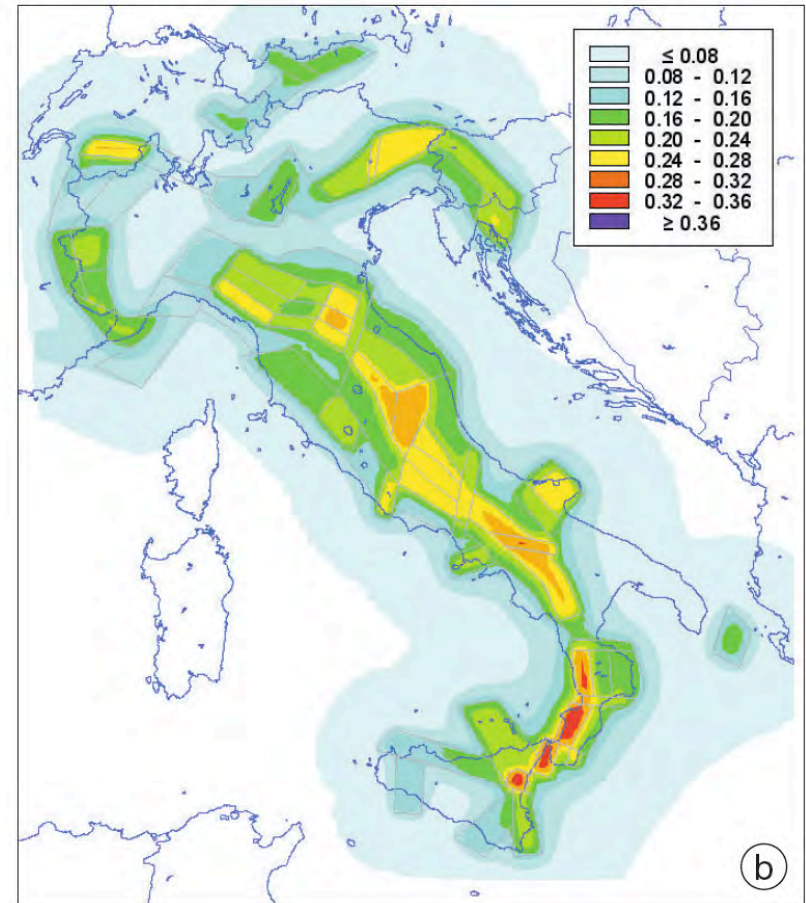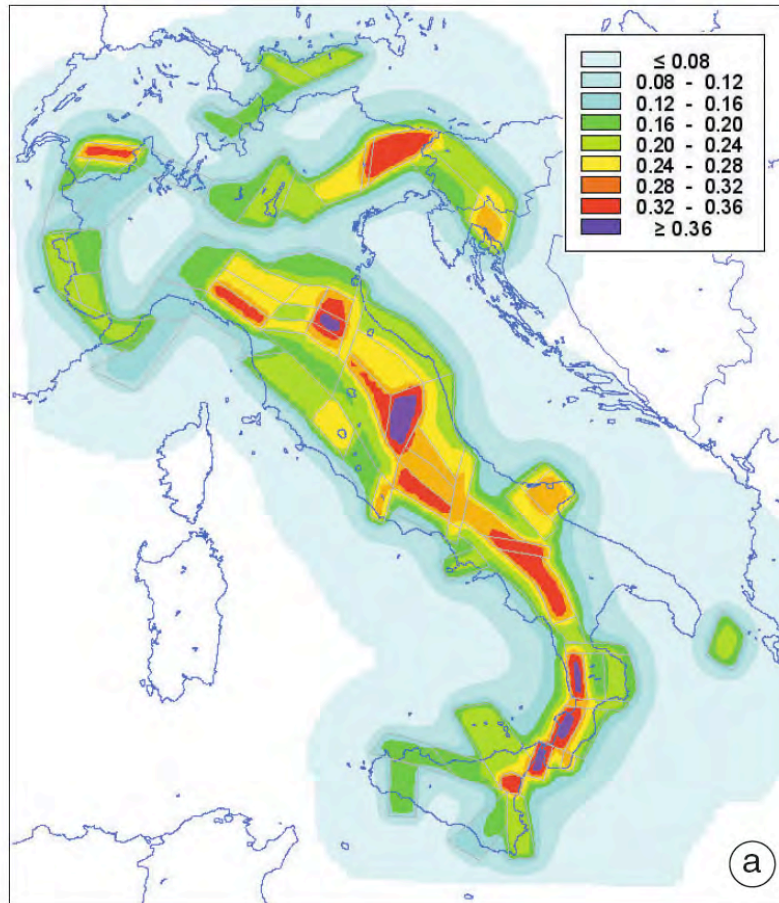
Stucchi et al 2004

**Fig. 11a,b.** Comparison of the PSHA obtained using distributions (a) VS2 of fig. 10 and (b) VS1, this paper, leaving unchanged all the other input data and using the same code to compute seismic hazard.

# PSHA: Probablistic Seismic Hazard Assessment Maps

Stucchi et al 2004

ISTITUTO NAZIONALE DI GEOFISICA E VULCANOLOGIA

Mappa di pericolosità sismica del territorio nazionale
(riferimento: Ordinanza PCM del 28 aprile 2006 n.3519, All.1b)

espressa in termini di accelerazione massima del suolo
con probabilità di eccedenza del 10% in 50 anni
riferita a suoli rigidi (Vs₃₀> 800 m/s; cat.A, punto 3.2.1 del D.M. 14.09.2005)

< 0.025 g
0.025 - 0.050
0.050 - 0.075
0.075 - 0.100
0.100 - 0.125
0.125 - 0.150
0.150 - 0.175
0.175 - 0.200
0.200 - 0.225
0.225 - 0.250
0.250 - 0.275
0.275 - 0.300

Le sigle individuano isole
per le quali è necessaria
una valutazione ad hoc

Elaborazione: aprile 2004

0  50  100  150  km

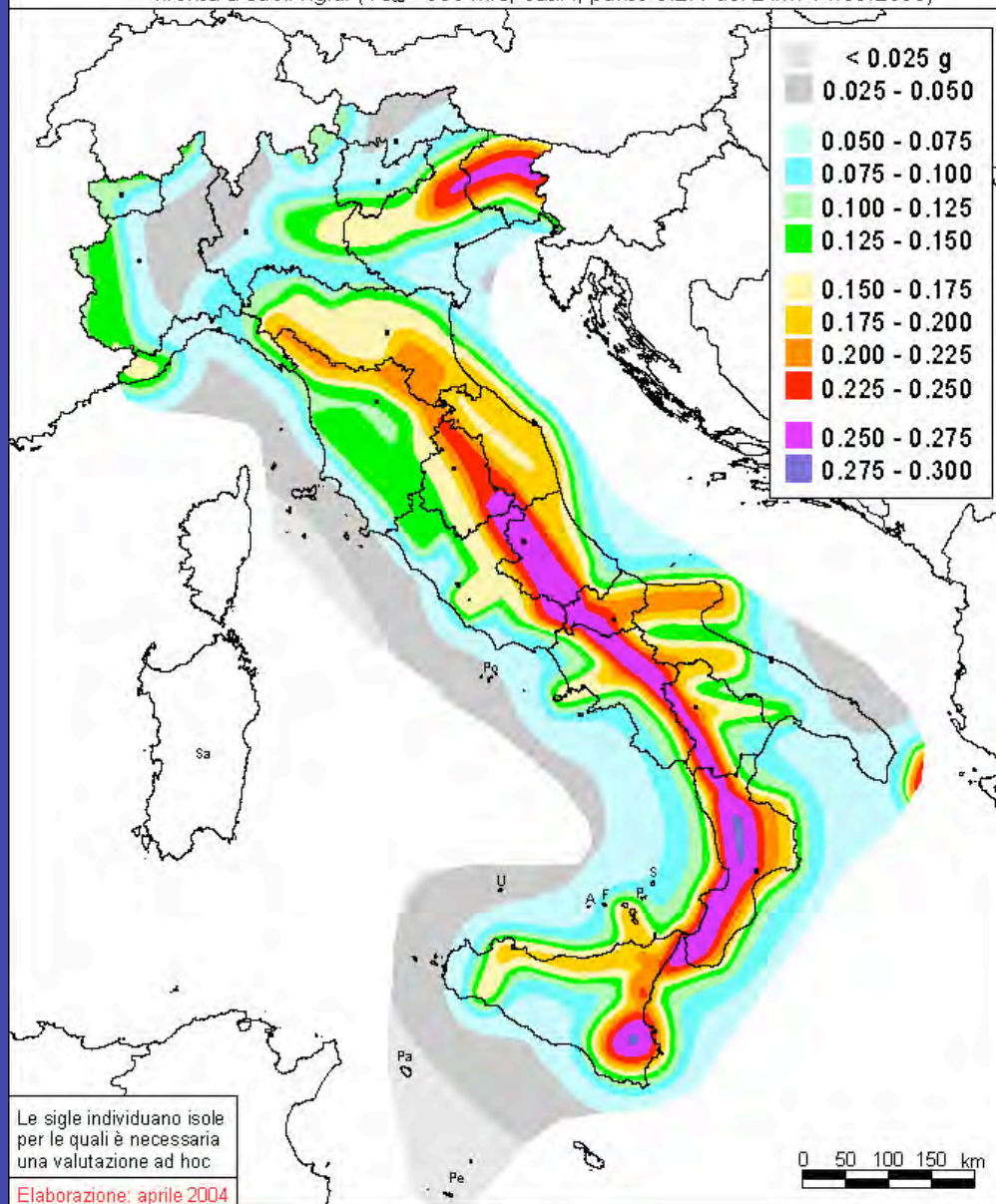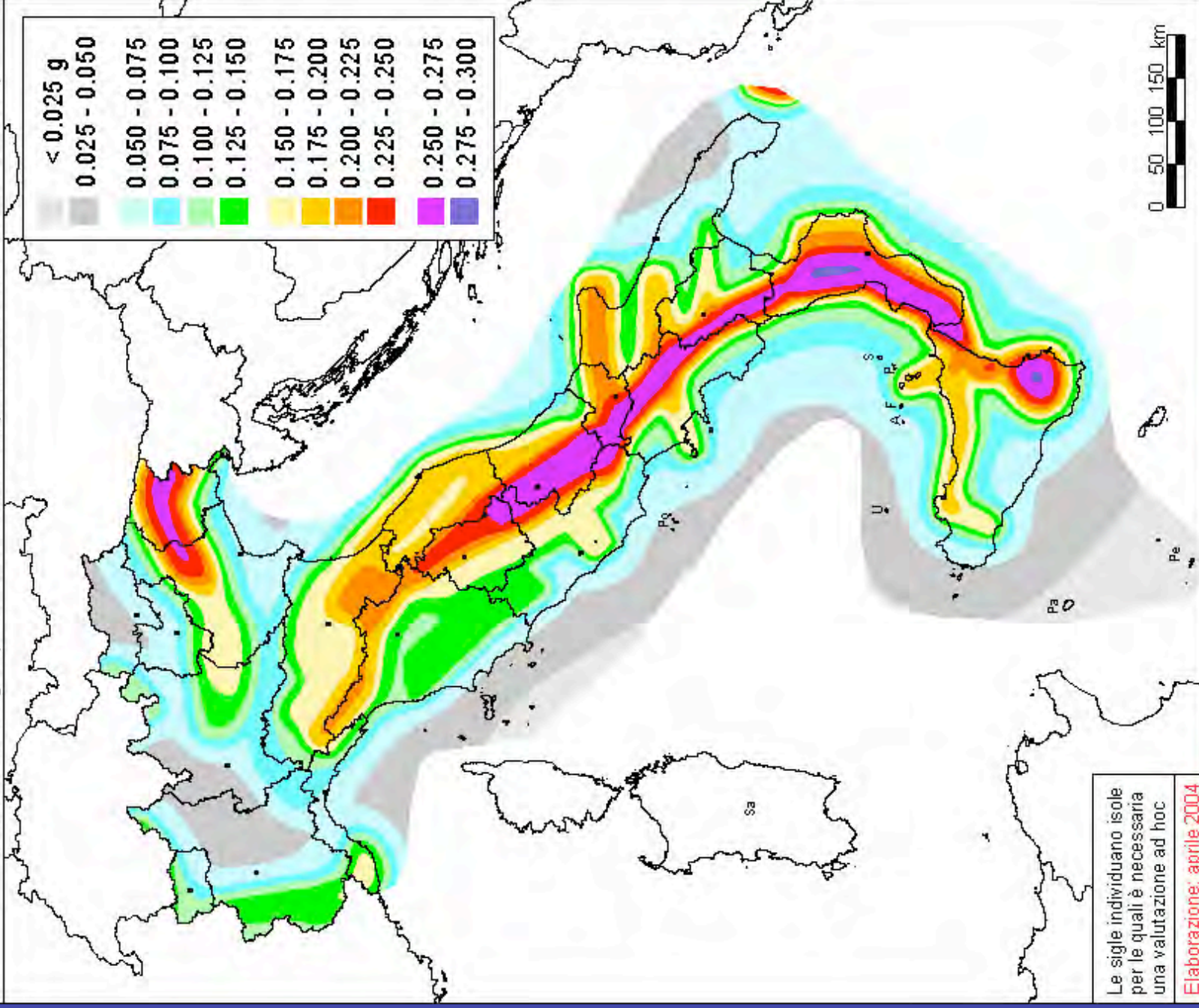# ISTITUTO NAZIONALE DI GEOFISICA E VULCANOLOGIA

## Mappa di pericolosità sismica del territorio nazionale

(riferimento: Ordinanza PCM del 28 aprile 2006 n.3519 , All.1b)

espressa in termini di accelerazione massima del suolo
con probabilità di eccedenza del 10% in 50 anni
riferita a suoli rigidi (Vs₃₀> 800 m/s; cat.A, punto 3.2.1 del D.M. 14.09.2005)



| | |
|---|---|
| | < 0.025 g |
| | 0.025 - 0.050 |
| | 0.050 - 0.075 |
| | 0.075 - 0.100 |
| | 0.100 - 0.125 |
| | 0.125 - 0.150 |
| | 0.150 - 0.175 |
| | 0.175 - 0.200 |
| | 0.200 - 0.225 |
| | 0.225 - 0.250 |
| | 0.250 - 0.275 |
| | 0.275 - 0.300 |

0  50  100  150  km

Le sigle individuano isole
per le quali è necessaria
una valutazione ad hoc

Elaborazione: aprile 2004